Nuclear Engineering and Design Volume 382 (2021), 111383
https://doi.org/10.1016/j.nucengdes.2021.111383

Preliminary uncertainty quantification of the core degradation models in predicting the Fukushima Daiichi unit 3 Severe Accident

Matteo D'Onorio, Alessio Giampaolo, Gianfranco Caruso, Fabio Giannetti
Dep. of Astronautical Electrical and Energy Engineering (DIAEE)
Sapienza University of Rome
C.so Vittorio Emanuele II 244, 00186 Rome, Italy

Abstract

A MELCOR model of a boiling water reactor has been developed by Sapienza University of Rome in the framework of the MUSA project aiming at identifying and quantifying uncertainty sources in severe accidents analyses. To develop the model, the Fukushima Unit 3 boiling water reactor has been taken as reference, and a preliminary sensitivity analysis with RAVEN software coupled with MELCOR has been performed to quantify the influence of core degradation parameters on selected key figures-of-merit, such as pressure vessel and containment pressures, core liquid level, hydrogen generation, lower head breach time and source term.
Results of base case satisfactorily predict main pressure and liquid level data measurement from TEPCO. As well as, results from the uncertainty analysis envelope the majority of thermohydraulic TEPCO reported measured data. Furthermore, median of calculated core status is in likely agreement with recent TEPCO containment inspections and muon measurements, with about 25% of fuel rods remained intact in RPV and 65% of core masses ejected to the pedestal.

Keywords: Boiling Water Reactor, MELCOR, RAVEN, Sensitivity, Uncertainty Quantification

1. Introduction

The great earthquake disaster hit the east coast of Japan at 14:46 on Friday March 11th, 2011. The earthquake damaged residences and industrial establishments, causing the immediate reactor SCRAM in the active units of the Fukushima Daiichi nuclear power plant. The subsequent tsunami wave flooded the lower parts of reactors 1-4, causing a complete loss of core reactor cooling. The Fukushima accident was the first world severe accident in a Boiling Water Reactor (BWR), offering, despite of the consequences, a unique opportunity to deepen the knowledge on core degradation phenomena and to improve abilities of severe accidents codes in modelling complex accident scenario.

Corresponding author: matteo.donorio@uniroma1.it

In past years, many efforts have been made to better understand the accident sequence (Gaunt et al., 2012; Fernandez-Moguel et al., 2019a; Sevón, 2015; Robb et al., 2014), the extent of damage (Pellegrini et al., 2016; TEPCO, 2017) and the end state of the reactor core (Pellegrini et al., 2019; TEPCO, 2017) at the Fukushima Daiichi Unit 3. Moreover, several benchmark studies have been performed to analyze and compare the accident progression using different severe accident codes (Lind et al., 2021; Pellegrini et al., 2016). However, although the significant advancements in modelling severe accident scenario, there are still open issues. In fact, some phenomena are very difficult to simulate. This lack of knowledge inevitably led to the adoption of a simplified severe accident treatment operated by computer codes. Furthermore, as extensively described in (Pellegrini et al., 2019), the Fukushima Daiichi Unit 3 severe accident was characterized by different layers of uncertainties, ranging from equipment functionality to the lack of knowledge about real accident progression, which makes even more complex and difficult to correctly reproduce different transient phases.

The purpose of this work is to perform a preliminary quantification of the uncertainties, focused on core degradation phase of the severe accident transient that occurred at Fukushima Daiichi Unit 3 nuclear power. For this, the impact on selected figures-of-merit (FoMs) generated by the MELCOR degradation model is investigated. The RAVEN software tools (Rabiti et al., 2017) coupled with severe accident code MELCOR 2.1 (Humphries et al., 2015; Humphries et al., 2017) has been used to evaluate the influence of input parameters on selected key FOMs.

The base case scenario has been simulated as well, using TEPCO data available in the literature and current Best Practice Guidelines given in SOARCA (Ross et al., 2014). Missing data plant, mainly related to the containment, were scaled from Peach Bottom Unit 2 plant, similar to the Fukushima Daiichi Unit 3 but larger in power (3514 MWt). A comparison of the obtained results with TEPCO reported data and on-site investigation has been performed to evaluate the influence of input parameters on selected key FoMs.

2. MELCOR model description

MELCOR is a State-Of-Art fully integrated modular computer code capable of performing severe accidents progression in LWR, developed at Sandia National Laboratories (SNL) for the U.S. Nuclear Regulatory Commission (U.S.NRC). Through different packages, the code can simulate the main phenomena characterizing severe accident transient as thermal hydraulic in primary system and containment, core degradation and relocation, aerosol release, transport and deposition.

The developed MELCOR nodalization includes main Reactor Pressure Vessel (RPV) components, Primary Containment Vessel (PCV) components and Reactor Building (RB). They have been modelled using the MELCOR Control Volume Hydrodynamics (CVH) package, responsible for modelling the thermal-hydraulic behaviour of liquid water, water vapor, and gases in MELCOR, giving boundary conditions to all other packages. Core and lower plenum structures, including their thermal response and relocation during degradation, melting, slumping, and debris formation, are modelled in the COR package. The bottom of RPV has been taken as the reference level (0 m).

The nodalization has been designed to have a reasonable computational time and a realistic prediction of the phenomena involved during the accident, assuring a reliable and accurate transient simulation. MELCOR

nodalization and models have been developed following the Best Practice Guidelines given in SOARCA (Ross et al., 2014) to better represent the plant response to the severe accident.

2.1 Core and in-vessel components nodalization

The MELCOR in-vessel model includes downcomer, recirculation loops, jet pumps, steam separators, steam dryers, steam dome and four steam lines, as well as lower plenum and core region.

In Figure 2 the COR nodalization is shown. Lower plenum and core structures have been modelled using 19 Axial Levels (AL) and 6 rings. The active core region has been represented by 4 concentric core rings with associated radial peak factors reported in Table 1 (TEPCO, 2013b). The fuel assemblies have been divided into ten axial levels (9-18th AL). Distribution of axial power peak factor is reported in Table 2 (TEPCO 2012a). The 5th radial ring model the annular region between active core and shroud, while the 6th simulates the reactor downcomer.

The 40 active core cells are thermally coupled two by two for each CV, modelling the power response of the included fuel assemblies, giving an accurate and continuous representation of the local fuel degradation. As shown in Figure 1, 20 CVs have been used to simulate four core channels and associated bypass volumes, connected through flow paths that open when the canister fails, allowing natural circulation in the open core after channel box failure. The Lower Plenum (LP) region has been divided into 8 axial levels, coupled with one control volume, CV900 in Figure 1. Each flow path in the core and lower plenum nodalization is allowed to simulate the effects of flow blockages and changes in resistance during core degradation.

Fukushima Daiichi Unit 3 was a BWR/4 of 2381 MWt. According to TEPCO data, when the accident occurred, there were 93 t of U, corresponding to 105.5 t of UO_2, contained in 516 Uranium dioxide 9x9 Fuel Assemblies (FAs) and 32 Uranium Mixed Oxide (MOX) 8x8 FAs. Masses calculated from geometrical data and used in the MELCOR input deck are reported in Table 3.

The operating pressure in the reactor pressure vessel was 7.03 MPa considering an average core temperature of 286 °C. Cooling water with a calculated steam quality of 14% enters in a common control volume from core CVs representing the core shroud head region, and from here moves to steam separators, steam dryer and four steam lines, discharging steam exhaust from RPV to a time-independent control volume simulating the main turbine. The used RPV nodalization scheme is shown in Figure 3.

Table 1 - Radial Peak Factor

Ring	**1**	**2**	**3**	**4**	**5**	**6**
FAs Number	124	136	144	144	0	0
Peak Factor	1.19	1.17	1.01	0.63	0.0	0.0

Table 2 - Axial Peak Factor

AL	**9**	**10**	**11**	**12**	**13**	**14**	**15**	**16**	**17**	**18**	**19**
Elevation (m)	5.30	5.67	6.04	6.41	6.78	7.16	7.53	7.90	8.27	8.64	9.01
Peak Factor	0.82	1.42	1.29	1.17	1.10	1.04	1.04	1.02	0.84	0.26	0.00

Table 3 - Main masses in MELCOR COR package

	Steel (Kg)	**Zircaloy (Kg)**	**Boron Carbide (Kg)**
Supporting Structure	34560	600	-
Non-Supporting Structure	20790	15900	960
Channel boxes	-	16300	-

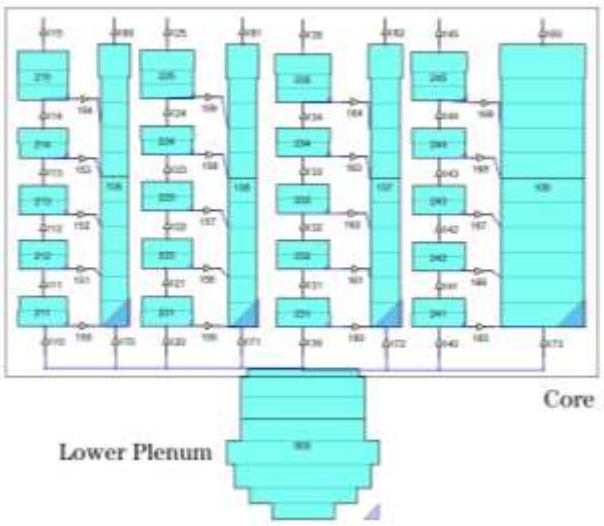

Figure 1 - CVH Lower plenum and core region nodalization scheme, made with SNAP

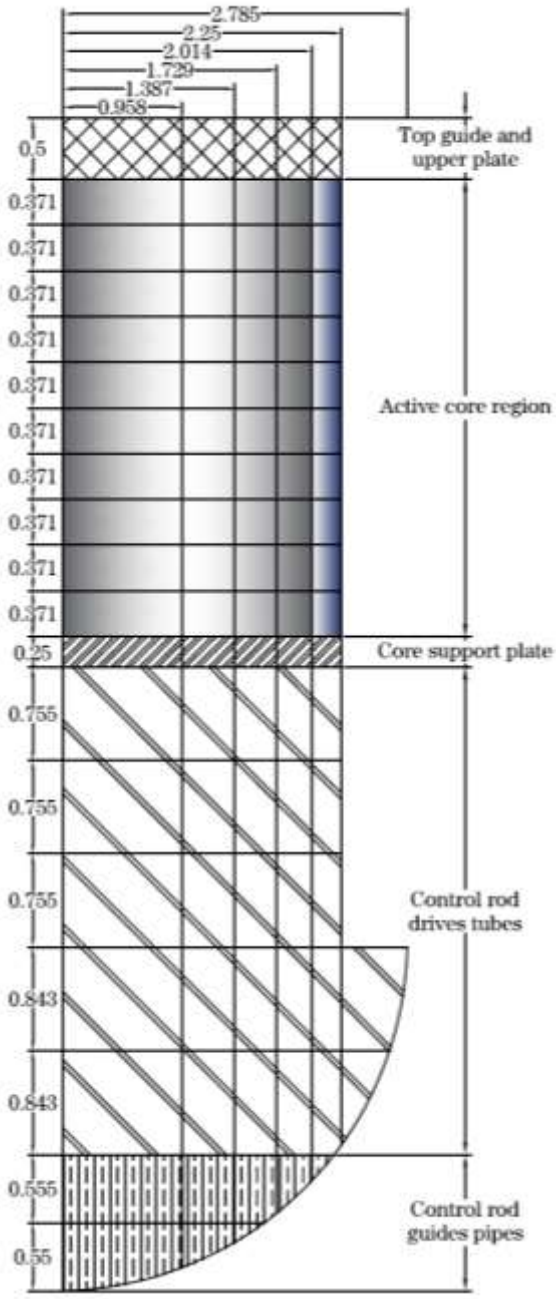

Figure 2 - COR nodalization

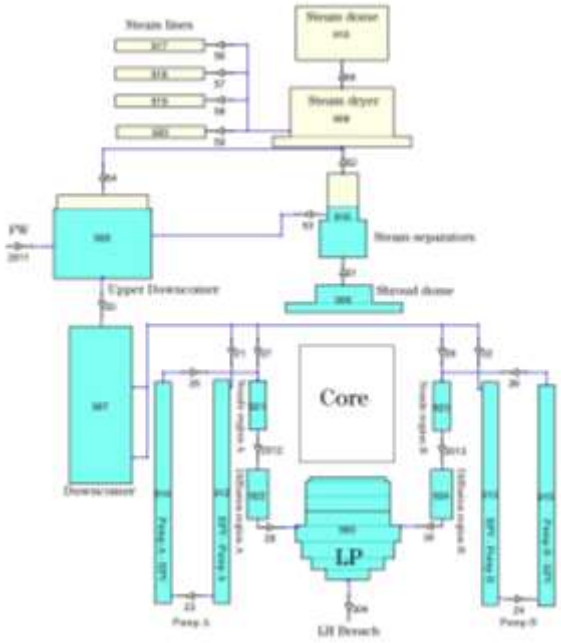

Figure 3 - RPV components nodalization scheme, made with SNAP

2.2 Primary Containment Vessel nodalization

The Primary Containment Vessel (PCV) model includes Drywell (DW), pedestal, vent lines, and Wetwell (WW). Pressure and temperature have been set respectively 0.106 MPa and 50 °C, due to stop of containment vessel cooling system (TEPCO, 2012a). The DW was connected to the WW with 8 vent lines, each composed of a vent pipe and 12 downcomers immersed in the suppression pool. Vent lines are also connected to the WW volumes through vacuum breaker flow paths, one for each vent line CV, which are assumed to open when the WW pressure exceeds the DW pressure by 3.4 kPa. The wetwell, a toroid shape suppression chamber, has been divided into eight sections according to SRVs exhausts in the suppression pool (TEPCO, 2013b). The WW had a

free volume of 3160 m^3 with a suppression water volume of 2980 m^3 (TEPCO, 2012a). As shown in Figure 4, each WW section has been modeled with two CVs connected with flow path, one simulating the bottom of the suppression pool (WWb – Wetwell bottom) and the other the upper water pool and the free chamber (WWt – Wetwell top). To avoid a complete suppression pool stratification when steam is discharged, a fictitious horizontal heat structure (1 mm thickness) has been inserted between the two different CVs. This also allowed to simulate natural circulation phenomena, since the code will calculate convection heat transfer from the WWt CV to HS and from the HS to WWb CV (Hoshi et al., 2013) (see Table 4).

2.3 Reactor Building

The Reactor Building (RB) model is shown in Figure 5. The torus room has been modelled as a single control volume. The reactor building floors 1-4 are associated to the same CV as the spent fuel pool and the fifth RB floor combined in the same CV. The decay heat power of 540 kW related to components stored in the spent fuel pool (TEPCO, 2013c), has been added as an enthalpy source in the spent fuel water volume of 1390 m^3. Environment and volume space between the DW head and the concrete shield plugs, have also been modelled. All initial conditions of RB control volumes have been set as atmospheric ones, 0.1013 MPa and 25°C.

Leakage from DW to RB location was assumed to be at the DW head, from the "shield volume" to the reactor hall. The leak area was increased linearly from 0.0 (at the atmospheric pressure) to 0.023 cm^2 at 0.71 MPa, giving a leak rate of around 0.5% of containment free volume per day at the design pressure 0.48 MPa (TEPCO, 2013b).

When DW pressure exceeds 3.6 bar, leak area is assumed to be linearly proportional to DW pressure, in agreements with DW pressure decreases after about 24 h. Hydrogen explosion occurred on March 14th at 11:01 (68 h and 15 min after the earthquake) in reactor building has been simulated through the MELCOR burn package, setting an igniter inside the reactor hall CV, which is triggered at the explosion time.

Fukushima Daiichi Unit 3 had two different sump cavities, but detailed information about their geometrical data are missing. Therefore, the MELCOR model has been based on public information about Unit 1 cavities (TEPCO, 2011). The Main cavity is related to the pedestal CV. Sump 1 and Sump 2 cavities are related to Sump CV. The concrete type in the Fukushima plant is basaltic and MELCOR's default concrete type CORCON basalt was used (Humphries et al., 2015; Humphries et al., 2017). After corium ejection, Molten Concrete-Core Interactions has been simulated in cavities.

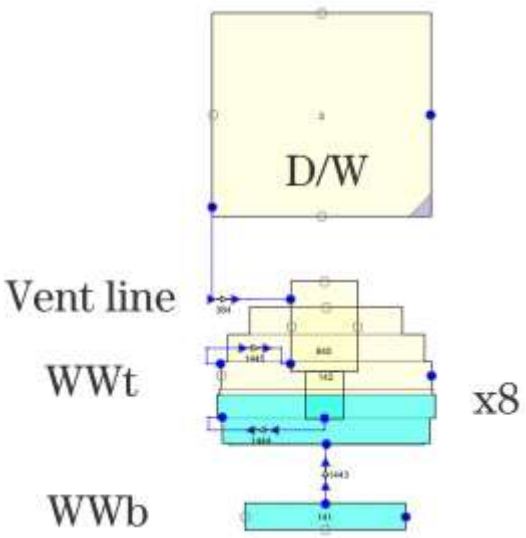

Figure 4 - WW nodalization

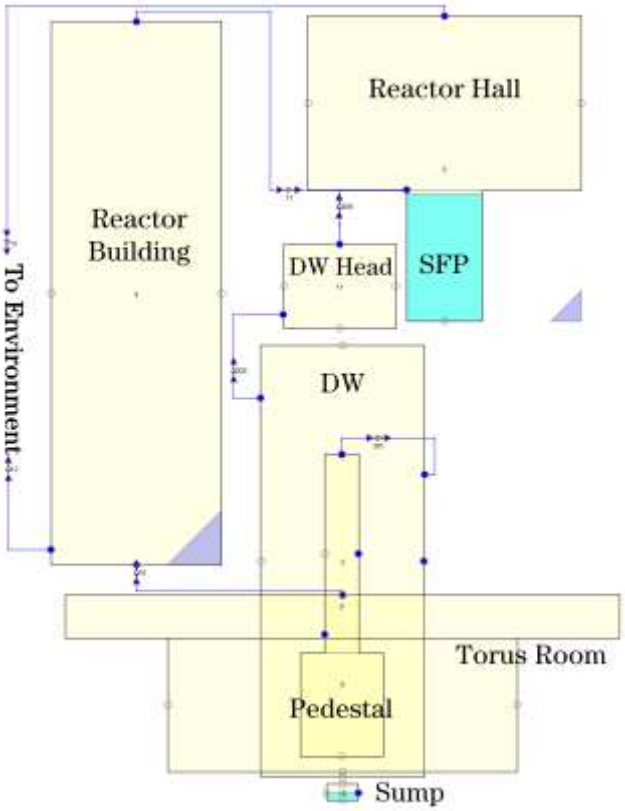

Figure 5 – Containment and reactor building volume nodalization

2.4 MELCOR models and assumptions

The MELCOR core degradation model is mostly based on loss of global support or local temperature exceeding the temperature-based failure criterion (Humphries et al., 2015; Humphries et al., 2017). Most of the input parameters related to core degradation are maintained with the default values. Some parameters such as molten Zircaloy breakout oxide shell temperature, maximum molten Zr breakout flow rate per unit width, effective temperature at which the eutectic formed from UO_2 and ZrO_2 melts have been modified as suggested in SOARCA best-practices (Bixler et al., 2016). Time-at-temperature criteria of fuel rods fail is introduced to avoid a cliff-edge effect of temperature threshold rod collapse.

Fuel response to high temperature standing involves complex phenomena like eutectic formation, swelling, Zircaloy melting and oxidation etc. A temperature-based criterion reflects many of these processes that affect fuel integrity, through an integral damage model representation of the fuel rods remaining lifetime: fuel rods conversion in particulate debris is triggered when the cumulative damage fraction is equal to one.

B_4C model is active, with B_4C melting temperature set to 1700 K, taking into account eutectic interaction with stainless-steel.

When core debris relocates from a position above the lower core support structures (slumping), direct interaction between over-heated or molten core debris and water pool occurs. Failure of penetrations (at temperature threshold of 950 K (Fernandez-Moguel et al., 2019b)) and vessel creep damage are calculated using a one-dimensional temperature profile through the lower head and Larson-Miller parameter.

At vessel failure, Molten Core-Concrete Interactions (MCCI) will take place in PCV with gradual erosion and ablation of the concrete basemat and reactor sump, leading to the gases release that increases containment pressure. Contact between the corium and any liquid water present in the reactor cavity could contribute an increase in the pressure inside the containment building. Contact between hot corium and colder concrete can lead to local formation of a crust by solidification. MCCI has been modelled in agreement with the MACE data (Ross et al., 2014).

Fission products have been divided into 17 radionuclide classes using JAEA ORIGEN calculation (Nishihara, 20212). MELCOR classes are chemically lumped except for the uranium class, or combinations of other radionuclide classes (e.g. CsI and Cs2MoO4). CORSOR-Booth high-burnup model was used for the releases from the core. Fission products are mainly in the condensed phase carried as aerosol particles, with the exception of noble gases. It has been assumed that all of the iodine is initially in the form of CsI. Caesium has been divided in gap inventory as CsOH in class 2, Caesium Iodide CsI in class 16 and Caesium Molybdate Cs2MoO4 in class 17. Decay heat at shutdown was 6.3% of full power rating, around 150 MWt (Cardoni et al., 2014b).

Table 4 - MELCOR radionuclides masses

Class ID	Class name	Representative	Initial inventory [kg]
1	Noble gases	Xe, Kr	347.8
2	Alkali metals	Cs, Rb	47.16
3	Alkaline earths	Ba, Sr	147.4
4	Halogens	I, Br	1.33
5	Chalcogens	Te, Se	32.27
6	Platinoids	Ru, Pd, Rh	229.9
7	Early trans	Mo, Tc, Nb	210.84
8	Tetravalent	Ce, Zr, Np	19241.56
9	Trivalent	La, Pm, Y, Pr, Nd	31.39
10	Uranium	U	93000
11	More volatile	As, Sb	0.96
12	Less volatile	Sn, Ag	287.73
13	Boron	B	-
14	Water	H_2O	-
15	Concrete	-	-
16	Caesium Iodide	CsI	27.04
17	Caesium-molybdate	Cs_2MoO_4	200.252

Table 5 - Relief and Safety mode opening pressure

	Relief Function		Safety Function	
	Opening P (bar)	**Closing P (bar)**	**Opening P (bar)**	**Closing P (bar)**
SRV C	*75.4*	*72.5*	*77.4*	*74.5*
SRV A, E, G	*76.1*	*73.1*	*78.1*	*75.1*
SRV B, D, F, H	*76.8*	*73.8*	*78.8*	*75.8*

2.5 Main Safety system modelling and operation

Main safety systems whose operation occurred during the accident scenario at Unit 3 of Fukushima Daiichi, such as Reactor Core Isolation Cooling (RCIC) system, High Pressure Coolant Injection (HPCI) system, overpressure protection and automatic depressurization system, containment venting, primary Containment Spray System (CSS), and Alternative Water Injection (AWI) system have been modelled in detail with MELCOR.

The RCIC and HPCI systems provide core cooling and supply make-up water to maintain the adequate water level in RPV. They work in same way, differing on flow capacity and operating pressure: steam is extracted from the steam line, driving a small turbine which runs a pump that supplies make-up water from the Condensate Storage Tank (CST) to the RPV in the feedwater injection line at the normal reactor operating pressure, while the turbine exhaust is discharged in the suppression pool. All the valves are driven by DC power from the batteries. Operation times of the RCIC and HPCI systems were taken from (TEPCO, 2012a), and they are reported in Table 7. The RCIC system operation is divided into two units. The first unit model simulates the steam flow from one of the four steam lines (SL) to one of the upper wetwell sections and consequently the turbine operation. The second unit model simulates instead the pump delivering water from the core storage tank (CST) to the RPV feedwater injection line. For the first RCIC operation steam extraction and water injection was set to nominal value (Pellegrini, 2014). During the accident the operators manually controlling steam extraction and the water injection to the RPV, through a test loop line, to save battery power and control RPV water level without repeated start and stop of emergency system, either from second RCIC operation and HPCI. The pressure response was dominated by steam extraction, the RPV water level was dominated by water injection to the RPV. To model RCIC system operation flow paths velocity and open fraction have been controlled through control and tabular functions. The mass flow rate of the steam through the turbine depends on the pressure difference between the RPV and WW and density of steam in the steam lines. In order to reproduce operators adjusted RCIC/HPCI water flow rate to RPV, injected water in model has been tuned according to response of measured water level.

The overpressure protection and automatic depressurization system (ADS) of the reactor pressure vessel were provided by Safety Relief Valves (SRVs), which were connected to four steam lines, discharging steam into the WW. The overpressure protection was achieved by the continuous SRVs opening and closing at a pre-set high and low RPV pressure. The relief function, which operated at a lower pressure than the safety one, was guaranteed by nitrogen pressure provided through AC power or by accumulators, while the safety function had spring force as drive source. The activation relief and safety valves pressures were different and summarised in

	Relief Function		**Safety Function**	
	Opening P (bar)	**Closing P (bar)**	**Opening P (bar)**	**Closing P (bar)**
SRV C	*75.4*	*72.5*	*77.4*	*74.5*
SRV A, E, G	*76.1*	*73.1*	*78.1*	*75.1*
SRV B, D, F, H	*76.8*	*73.8*	*78.8*	*75.8*

.

According to the Unit 3 recorded charts provided in (ICANPS, 2012), during the period from the earthquake until the tsunami hit, SRV-C (which had the lowest relief function working pressure) repeatedly opened and closed through nitrogen pressure provided by AC power. However, at 15:38 on March 11th, AC power was loss, causing the nitrogen pressure supply piping closure. From this point, the required nitrogen pressure for opening started

coming from accumulators, ensuring relief function only for eight movements per SRV, until nitrogen pressure inside accumulators was consumed. After all the SRVs trains operated 8 times in relief function, the safety operation has been simulated and allowed until the ADS occurred. After the HPCI stopped, the ADS actuated by operators has been modelled through the opening of 2 equivalent SRVs areas at depressurization time (42 h 10 min after earthquake).

The purpose of the containment venting system is consequently to avoid overpressure in the PCV to protect and maintain the integrity of the containment preventing the possibility of a direct and uncontrolled release of radioactivity to the environment. Vent paths include a train from DW and a main one from the WW, in order to benefit of radionuclide scrubbing removal by pool. Referring to accident events, a Motor Operated (MO) valve manually opened to 15% at 08:35 on March 13th, while an Air Operated (AO) valve opened and closed several times. The venting line can start its function when the rupture disk burst, at the activation pressure of 528 kPa (ICANPS, 2012). The MO valve operation was not modelled, while rupture disk and AO valve have been simulated. Despite of the big uncertainties related to venting line operation, the developed MELCOR model is based on TEPCO assumed venting system interventions (TEPCO, 2012d).

The primary Containment Spray System (CSS) is used to cooldown and depressurize the WW and the DW volumes, driving water from the suppression pool or the CST to the dry containment or to the upper non-pool section of the WW. The MELCOR model of the containment spray system is shown in Figure 6. During the accident sequence the spray system operated using the Diesel Driven Fire Pump (DDFP): TEPCO analysis evaluated a mass flow rate of 13.8 kg/s as the maximum flow rate elaborated from the DDFP. Water injection flow rates have been modelled as boundary condition, DDFP mass flow rates are assumed constant during spray system operation, as shown in Figure 7. Operation times of the sprays were taken from (TEPCO, 2012b).

Water was injected in the RPV by AWI through fire engines. The entire volume of alternative water injected by fire engines seems unlikely that was discharged into the reactor. There is the possibility that part of the discharged water was instead sent to other systems and equipment. As reported in Table 6 there was a significant difference between discharged and TEPCO RPV injected water by fire engines. The RPV injection through fire engines has been simulated with a flow path from the CST CV to the upper downcomer CV. Injected water temperature has been assumed at 10°C.

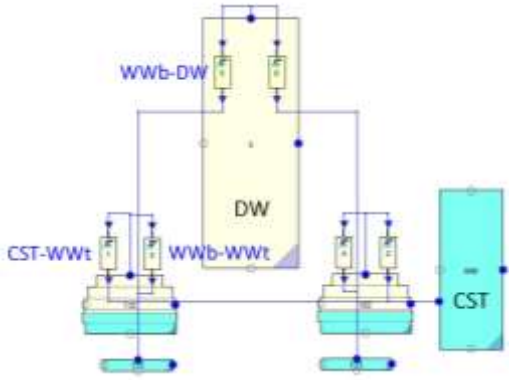

Figure 6 – Primary Containment Spray System, SNAP view

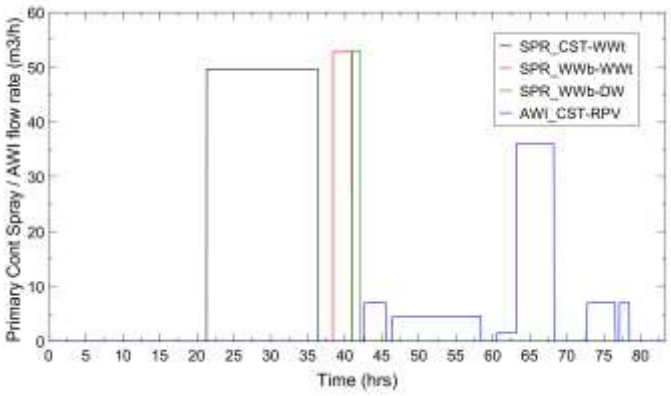

Figure 7 – CSS and MAAP analysis-injected flow rate into RPV

Table 6 - Water flow rate injected by fire engines

Time (Duration)	Injected in RPV	Mass
hh:mm	t/h	t
42:25 - 45:34 (02:55)	7	20.4
46:26 - 58:24 (11:58)	4.5	53.8
60:34 - 68:15 (07:41)	1.5 (1/3 time) 36 (2/3 time)	188.2
72:44 - 76:34 (03:50)	7	138
77:08 - 78:28 (01:20)	7	9.333

3 Base case Accident Analysis

The summary of events assumed and modelled in the MELCOR simulation is reported in Table 7. Most times are based on TEPCO reported data, while some are modified to better represent accident behaviour. Initial conditions of the transient are given by a 2000 s steady state MELCOR calculation. Values are in good agreements with reference operational status. MELCOR calculation results have been compared with public measured data taken from (TEPCO, 2012b) and (TEPCO, 2012c). Simulation results are analyzed in the following sections at different accident phases.

Table 7 - Accident events timeline

Time after earthquake hh:mm	Event
00:00	Earthquake, SCRAM, loss of offsite power, start of DDFPs and isolation of RPV
00:19 – 00:39	I° RCIC operation
00:52	Tsunami and SBO
01:17 – 20:50	II° RCIC operation
21:20 – 36:19	Spray CST to WW
21:49 – 35:56	HPCI operation
38:22 – 40:57	Spray WW to WW
40:57 – 42:04	Spray WW to DW
42:10	ADS and Vent line rupture disk burst
42:34 – 44:31	I° PCV vent operation
42:39 – 45:34	I° AWI water injection
45:44 – 47:44	II° PCV vent operation
46:26 – 58:24	II° AWI water injection
53:45 – 58:43	III° PCV vent operation
60:34 – 68:15	III° AWI water injection
68:10 – 68:15	IV° PCV vent operation
68:15	Hydrogen explosion
72:44 - 76:34	IV° AWI water injection
73:54 - 78:18	V° PCV vent operation
77:08 - 78:28	V° AWI water injection

3.1 From SCRAM to RPV depressurization

After the earthquake, the automatic reactor protection system successfully acted. The reactor SCRAM occurred on March 11th 2011, at 14:47, considered as starting time (0.0 h) for this analysis. As well known, the earthquake damaged the electricity transmission system between the NPP and external facilities, causing the total loss of off-site power. Emergency Diesel Generators (EDGs) started automatically at 1 min in response of loss of all off-site power, restoring AC power. Meanwhile, the RPV was isolated through the closing of Main Steam Line Isolation Valves (MSIVs). Consequently, the reactor pressure increased due to the continuous steam generation, until the SRV-C opened at the pre-set opening pressure of 7.54 MPa in relief function at 5 min and started to cycle maintaining the reactor pressure between accepted values discharging steam in the WW (Figure 8). After that SRVs consumed nitrogen accumulators' reserves for the relief function, safety function SRVs operation was established, with RPV pressure ranging from 77.4 bar to 74.5 bar of SRV-C. As shown in Figure 9, SRVs operation caused a pressure increase in WW and at about 23 min from SCRAM vacuum breaker opened.

After 52 min from the SCRAM, the tsunami generated by the earthquake flooded in the NPP's site, making totally unavailable the seawater pumps and diesel generators, with loss of emergency AC power and SBO. The damages of the tsunami were not only to power supplies, but also to buildings, machineries, and equipment installations, causing extremely difficult access and movement within the plant, precluding the immediate and continuous injection of water through alternative systems. Without make-up water provided by RCIC and the continuous operation of SRVs, the RPV water level started to decrease again (Figure 10). Consequently, at 1 h 17 min, operators from the main control room reactivated the RCIC system using DC power, which remained available in the Unit 3. Operators tried to avoid excessive power consumption by disconnecting lightning and non-safety instrumentation and mainly distributing the RCIC injection pump flow into RPV and, through a test loop line, back into the CST, in order to prevent the continuous automatic stop of the emergency system at high reactor water levels and automatic restart at low water level, avoiding excessive battery depletion due to repeated RCIC de-activation and re-activation, also ensuring stable reactor water levels. To reproduce with MELCOR the actions provided by operators, RCIC flow rate to RPV and injected water from RCIC have been tuned according to the response of water level. The assumed steam extraction rate from RPV and water injection rate from CST to RPV are shown in Figure 11. Moreover, recirculation pumps seals leak has been assumed at 6 h 5 min to better represent increasing of WW/DW pressure (Cardoni et al., 2014a; Sevón et al., 2015). At 20:36 reactor water level sensors became unavailable due to the loss of DC batteries, which were restored at 03:51 on March 13th, at 37 h 5 min after the earthquake, using batteries from the Hirono Thermal Power Station.

RCIC stopped automatically 20 h 50 min after the SCRAM, probably due to electric trip caused by high turbine exhaust pressure. Because of the 20.5 hours of operation of RCIC, WW pressure and temperature increased, forcing operators to activate WW spray systems (at 21 h 20 min.) through DDFPs in order to cool and stabilize WW pressure (Figure 9).

After 21 h 49 min from the SCRAM the HPCI system automatically started after the water level reached the low set point, causing a great depressurization of RPV because of the large capacity of the emergency system. The RPV depressurization led to pressure values at the HPCI turbine inlet below its design range. The possible

turbine damages and the consequent generation of a release flow from the RPV to the PCV forced operators to manually stop the HPCI at 35 h 56 min, since the automatic shutdown for low RPV pressure (8 bar) did not occur.

RPV pressure started increasing and at 36 h 19 min, when operators decided to use DDFP to provide make-up water to the reactor, by switching them from the WW spray line to the RPV injection line. However, the discharge pump pressure was not sufficient to exceed RPV pressure and no safety injection occurred. Without core cooling system, operators tried to restore the injection through HPCI system at 36 h 49 min, but the restart attempts were unsuccessful, carrying to the continued increase of RPV pressure, which exceeded 70 bar at 37 h 44 min (Figure 8). The DDFPs that were previously connected to the RPV injection line were changed back to the WW spray injection at 05:08 (38 h 22 min). At this point, the only way to cool the core was through fire engines, and at 05:21 works started to establish a line for seawater injection into the Unit 3 RPV from the backwash valve pit. At 06:30 there were two fire engines at the Unit 3 complex, one dispatched from Units 5-6 and one arrived from the Fukushima Daiini NPP. The seawater injection line was completed at 07:00, however its operation was delayed by the Site Superintendent as a result of a TEPCO headquarters communication which signalled to continue fresh water injection, if available, rather than sea water. The line was consequently changed to a borated fresh water source.

At 07:39 (40 h 43 min), CSS was switched from WW to DW, starting DW spraying at 07:43 (40 h 57 min) until about 08:50 (42 h 4 min). At this time spray line was changed to core injection line, but since the AC power had not been restored, HPCI injection was impossible, forcing to use AWI as the only reactor cooling system.

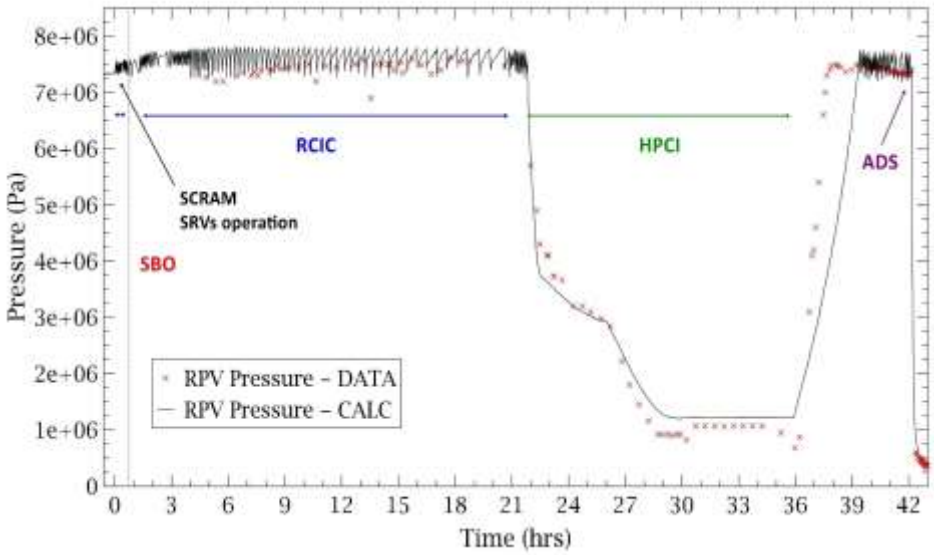

Figure 8 - RPV Pressure during RCIC operation

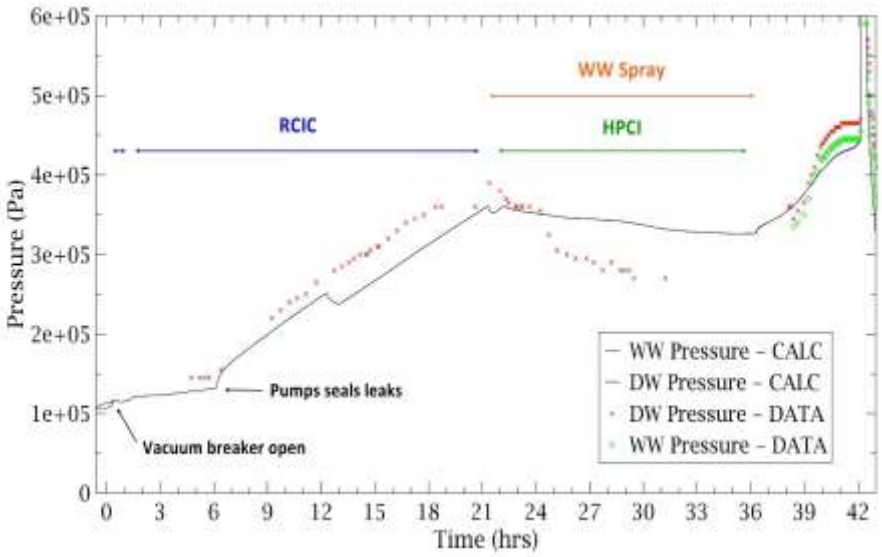

Figure 9 - DW/WW Pressure during RCIC operation

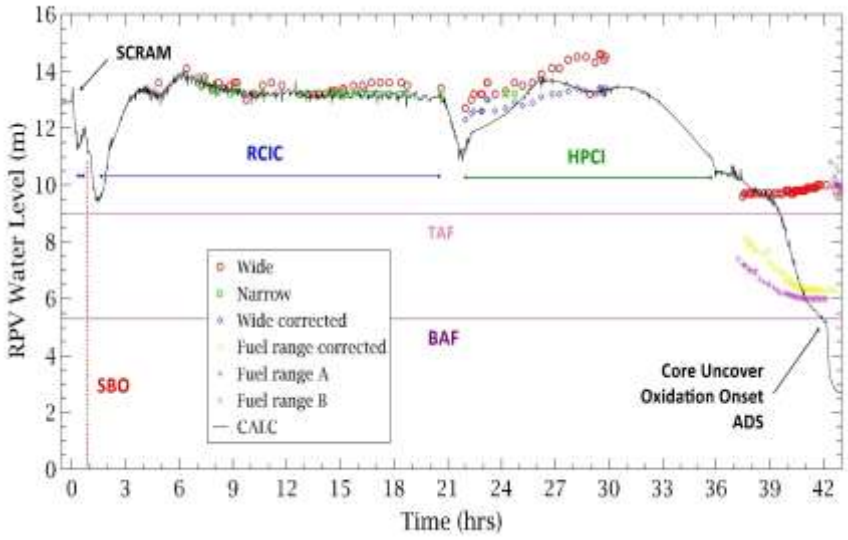

Figure 10 - RPV water level during RCIC operation

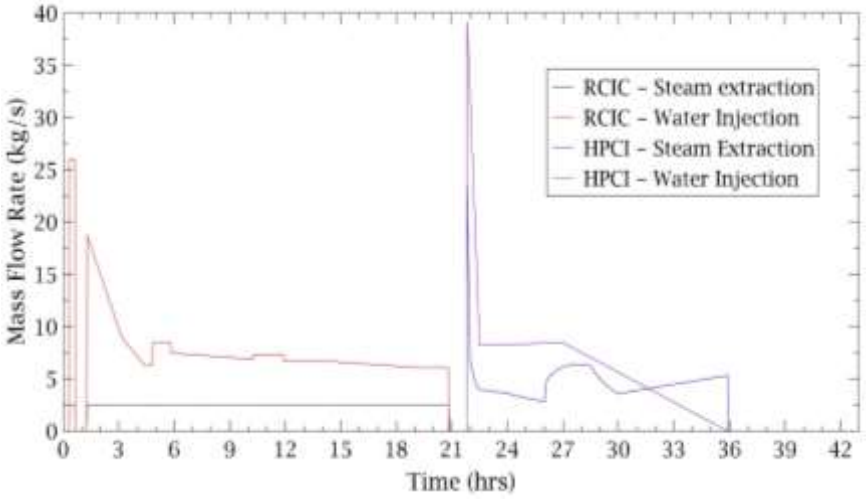

Figure 11 – RCIC and HPCI assumed mass flow rates

3.2 Core degradation and later accident phases

To guarantee AWI injection, the RPV should be depressurized and operators, using batteries gathered from cars, opened SRVs (2 SRV are assumed open in calculation) causing a drop in the reactor pressure at 42 h 10 min. During the depressurization of the reactor, a pressure peak was noticed in the PCV, causing a pressure increase in the WW carrying to the venting line rupture disc to burst (6.3 bar) after 42 h 34 min and the consequent PCV venting operation starting until 11:17 (44 h 31 min) when a valve on the vent line spuriously closed.

After the depressurization, borated freshwater injection started at 09:25 (42 h 39 min) until the complete tanks were empty (45 h 34 min). Consequently, the Superintendent decided to start seawater AWI through the line completed hours before. The fire engines were repositioned, the seawater AWI line restored and at 13:12 (46 h 26 min) the injection started.

Due to ADS operation, a high degree of steam production occurs in RPV that causes water level decrease from 5.2 m to 2.6 m. Furthermore, high steam flow causes a high core cooling, lowering its temperature from 2300 K to 1400 K (Figure 15). After depressurization, two pressure spikes can be observed in RPV: the first minor spike at 43 h 05 min rising about to 10 bar; and the major second spike at about 45 h 14 min of about 30 bar. Pressure spikes timing is in good agreement with TEPCO pressure strip data chart provided in (TEPCO, 2013a).

This is unlikely that these spikes are due to any SRV closing because they are characterized by a sharp increasing. Same spikes are on DW/WW pressure data, as shown in Figure 14. Furthermore, RPV water level data show large oscillations from 43 h to 46 h. From this evidence, it is strongly plausible and likely that pressure and level behaviour are caused by core degradation phenomena, like corium slumping and hydrogen generation.

Calculation results are in good agreement also with the second pressure peak. MELCOR predicts a RPV pressure peak of about 16 bar at 45 h 24 min. This is likely due to corium slumping in the lower head. In fact, core degradation started in MELCOR calculation at 41 h 33min, at the onset of hydrogen generation by cladding oxidation when clad temperature reaches 1100 K (Figure 15). Few minutes later, MELCOR predicts a first radionuclides release from gap due to clad failure. As shown in Figure 16, after 45 h 22 min from SCRAM a great portion of core collapsed, slumping in lower plenum and producing high vaporization and oxidation that causes pressure peaks in RPV and WW/DW. Core continues to gradually collapse from inner to outer parts and from top to bottom. At about 49 h, 60% of the core has collapsed (Figure 16) and slumped in lower plenum, producing other smaller pressure peaks. The first peak was not predicted by this MELCOR model, but it can also be related to core degradation phenomena (see Figure 17).

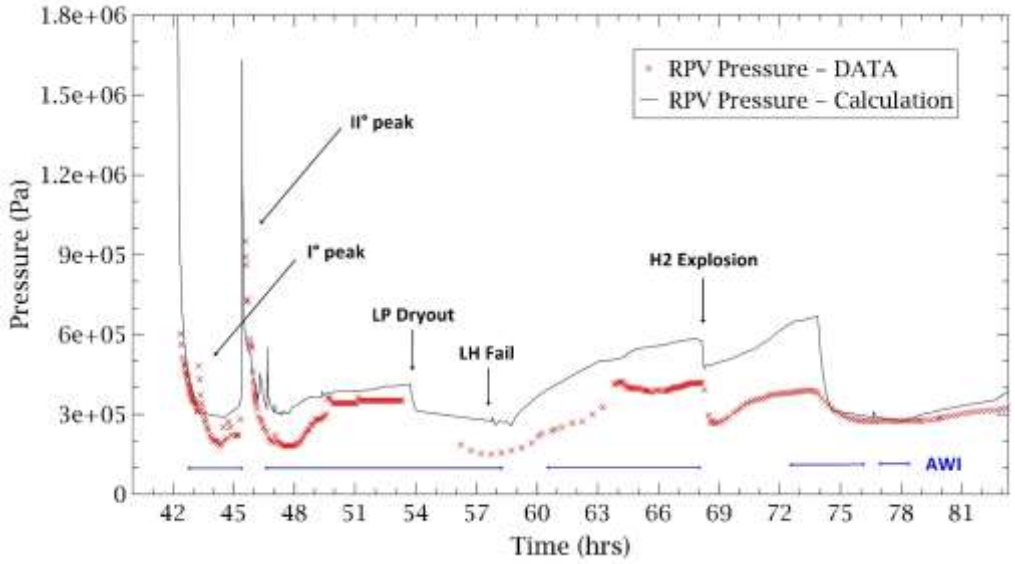

Figure 12 - RPV Pressure depressurization

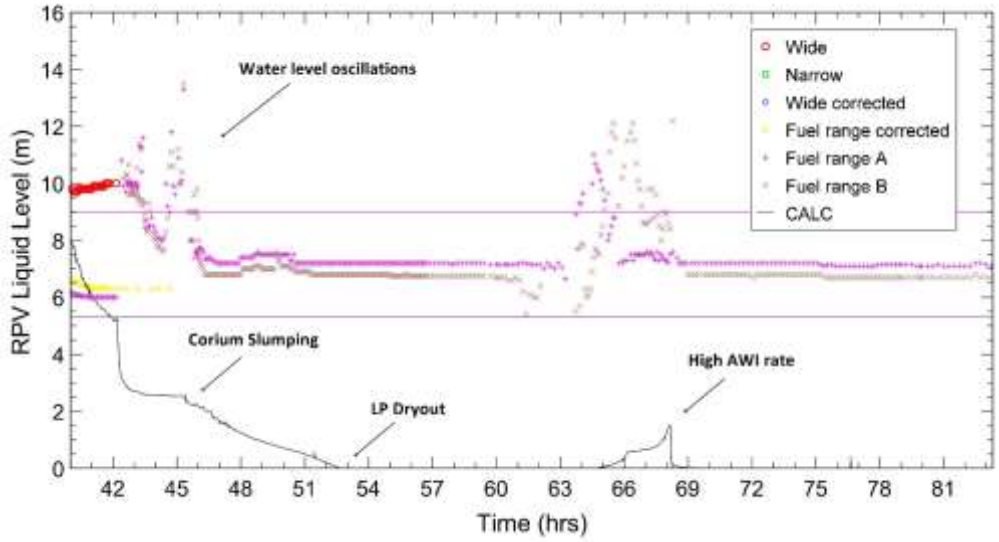

Figure 13 - RPV water level from depressurization time

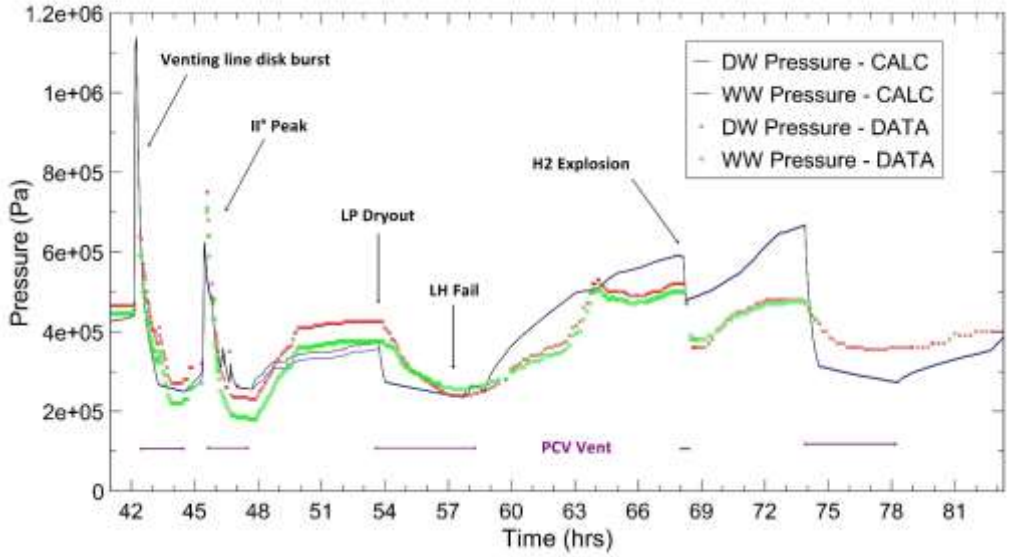

Figure 14 - DW/WW Pressure from depressurization

When corium is calculated to slumping into lower head, its water level is predicted to be about 2.6 m. Due to high vaporization, lower plenum water level begins to decrease, till lower head dryout predicted at 52 h 30 min (Figure 13). As shown by the pressure measurement data in Figure 12, the RPV pressure has a decreasing tendency from 53 h 30 min to 56 h 10 min, when pressure data measure 3.5 bar to 2 bar, although data missing between. Also, DW and WW pressure data show pressure decrease from 54 h to 57 h. This suggests lower steam production within lower head, likely due to no water present anymore, that means dryout time within these time value (Sato, 2017). MELCOR calculation predicts dryout few hours before indeed, but in general it is in good agreement.

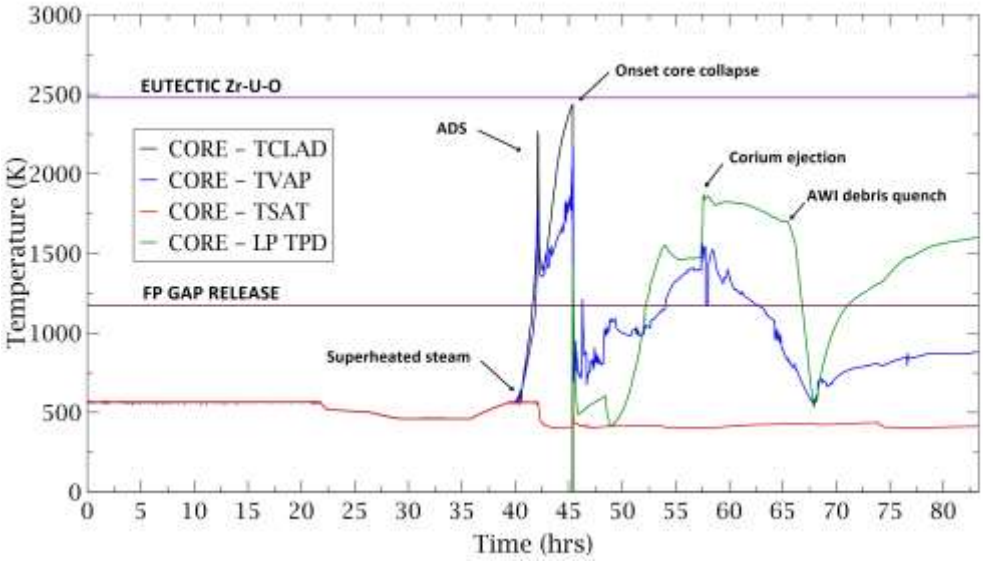

Figure 15 - COR Temperatures and degradation thresholds

Concerning WW/DW pressure behaviour, reported in Figure 14, the first pressure peak predicted to be 11.5 bar was caused by depressurization of RPV, discharging steam and non-condensable gases in WW from steam line by ADS and from WW to environment through stack venting line rupture disk. The first pressure peak after RPV depressurization was not predicted by this MELCOR model. The second one shows a good agreement with data, with a peak of 6.2 bar at 45 h 28 min, followed by lower peaks corresponding to gradual core parts slumping in lower head. At the end of calculations, about 75% of fuel has collapsed and 25% is still intact, resting in outer core region of the RPV characterized by a low power factor. The seawater injection continued until 01:10 (58 h 24 min) when it was halted since the pit water level decreased to an excessive low level. The injection restarted two hours later after the pit refill and the intake hose was lowered deeper inside the pit.

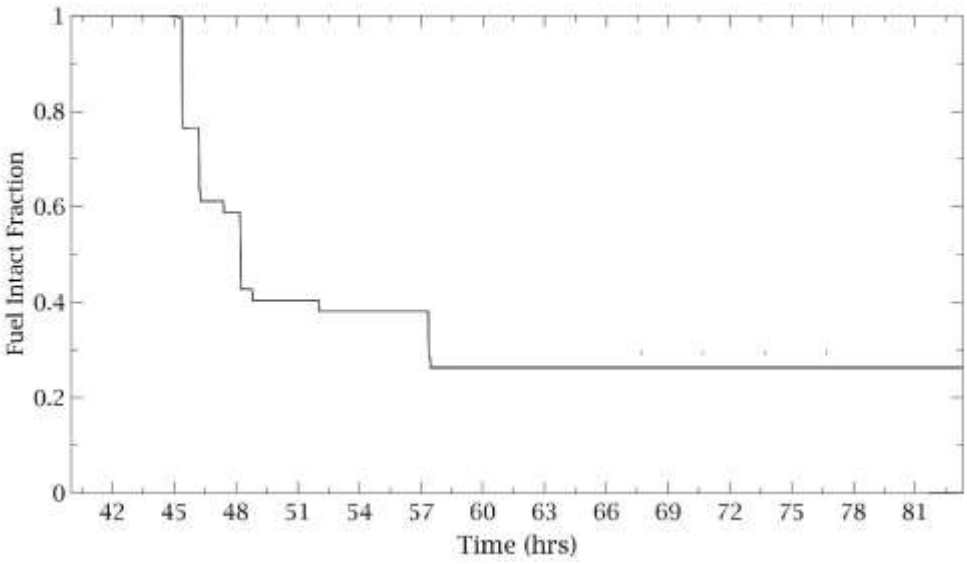

Figure 16 - COR degradation: Intact fuel fraction

3.2 Hydrogen generation and lower head failure

At 11:01 (68 h 15 min) an explosion occurred in the Unit 3 Reactor hall, injuring workers and damaging hoses and fire engines, causing the interruption of seawater AWI in Unit 2 and 3 and delaying operations in the Unit 1.

At time of explosion, core degradation has produced about 919 kg of hydrogen in MELCOR calculation. Hydrogen generation start at about 41 h 30 min, with first oxidation heat generation peak, and continues till corium slumping in lower plenum, with second oxidation peak, as shown in Figure 18. Hydrogen was probably escaped from DW to Reactor Hall trough head flange, weakened due to high differential pressure. MELCOR model calculates about 100 kg hydrogen leaked to reactor Hall at the time of explosion, close to that calculate to being necessary to cause hydrogen explosion in Fukushima Unit 1 of 130 kg (Yanez et al., 2015). Calculated H_2 mole fraction is 0.066 at time of explosion, with O_2 mole fraction of 0.137 in the reactor hall control volume.

Penetrations reach the threshold fail temperature of 950 K at 54 h 37 min (Figure 19). Because of constraint to minimum mass to be ejected, at this time no corium mass is assumed to be ejected by MELCOR. Lower head, however, can be assumed breached at this time. Vessel lower head fails by creep at 57 h 46 min. The total mass ejected is presented in reported in Table 8**Errore. L'origine riferimento non è stata trovata.**. The calculation ends after the main accidental events, when the reactor was maintained in stable conditions through the continuous water injection by fire engines and the restoration of offsite AC power. At this point (83 h 20 min) the total mass ejected from the RPV predicted by MELCOR is around 126,000 kg, composed by 65.8% UO_2, 11.1% SS, 4.6% SSOX, 7.3% Zr, 10% ZrO_2, 1.2% B_4C and Inconel (see Figure 20).

Main materials masses ejected to PCV and retained inside the RPV are summarised in Table 8, while calculated main states of reactor core degradation are illustrated in Figure 21. After the lateral breach of LH, part of the corium is discharged into PCV pedestal causing additional water vaporization. MELCOR predicts a water level of 2.74 m above pedestal floor at lower head fail. According to this calculation, MCCI start after 1 h 39 min

corium ejection. The basemat concrete ablates 1.85m net radius and 0.89m in height in sumps at the end of calculation, but it was still ongoing.

Under high radiation levels, seawater injection restarted at 15:30 and it was stopped at 02:30 on March 15th to provide water injection for Unit 2. These are the main events occurred in the first days after the earthquake. On March 15th 2011, five days later the beginning of the accident, the electricity was restored and continuous attempts to refill the spent fuel pool (SFP) and to inject fresh water to the reactor were carried out.

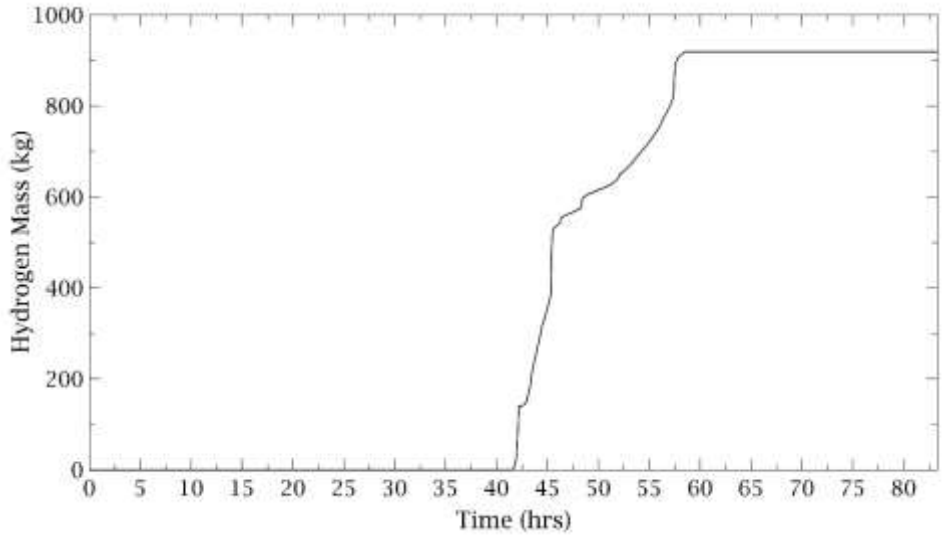

Figure 17 - Hydrogen generation due to core degradation

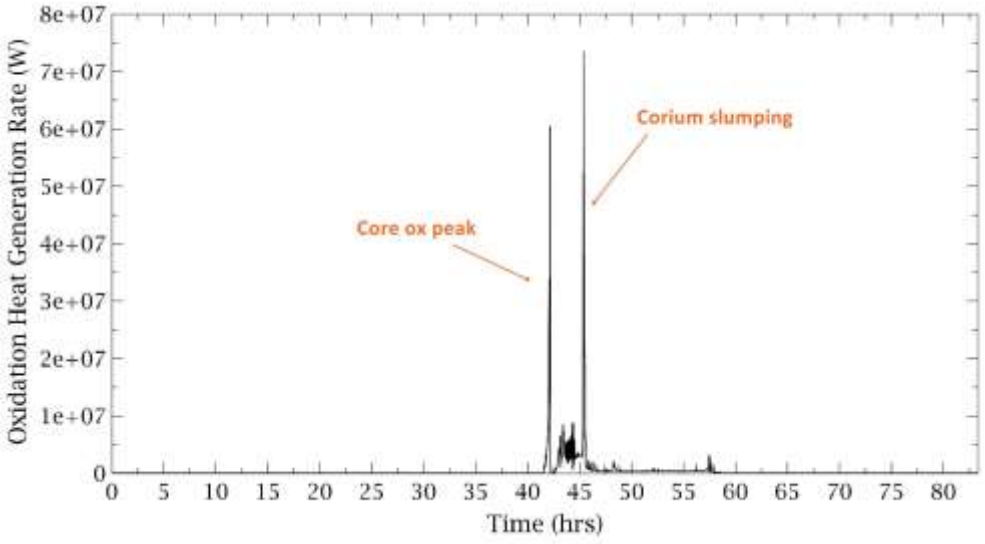

Figure 18 - Oxidation heat generation rate

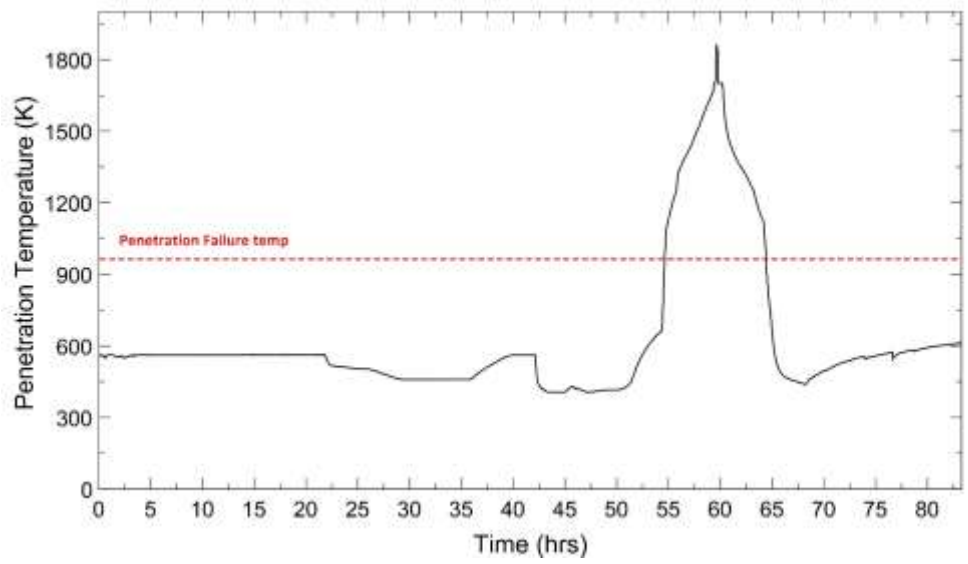

Figure 19 - Lower head penetrations fail temperature

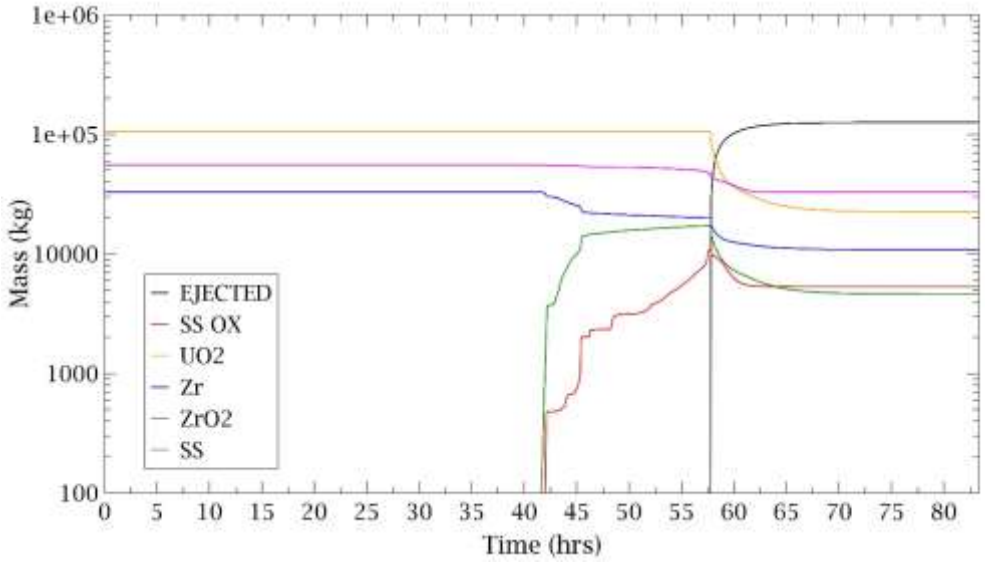

Figure 20 - Masses ejected from vessel breach

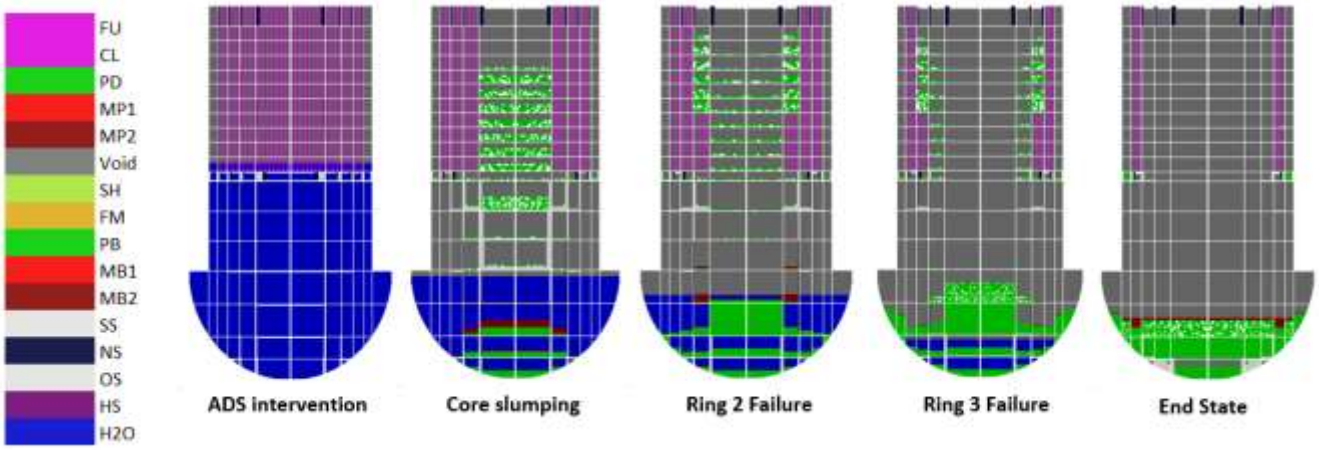

Figure 21 - Core degradation main states

Table 8 - COR masses ejected and retained

Material	Masses before ejection	Ejected fraction
UO2	105.5 t	78.6%
SS	46.9 t	30%
SSOX	11 t	52%
Zr	20.1 t	45.9%
ZrO2	17.2 t	73%
TOT	200.7 t	62.8%

3.3 Source term predicted by MELCOR

In the developed MELCOR model, leak paths from the main reactor buildings toward the external environment consist of 3 possible ways:

- venting line from WW to stack;
- reactor Hall to environment caused by explosion;
- containment leakage.

Total mass flow rates of gas released to the environment are presented in Figure 22. It should be noted that most of the source term is released through the unfiltered venting line path, although scrubbed through WW water.

The mains radionuclides considered for the present source term analysis are noble gas, caesium (in the chemical form of CsOH, CsI and Cs2MoO4) and iodine (in the chemical form of CsI). Except for the noble gases, the fission products are predominantly in the condensed phase carried as aerosol particles. Noble gases are not retained in the suppression pool water, and therefore they were almost totally released to the environment, with 98% of the initial inventory (i.i.) released in the environment at the end of calculation (Figure 23).

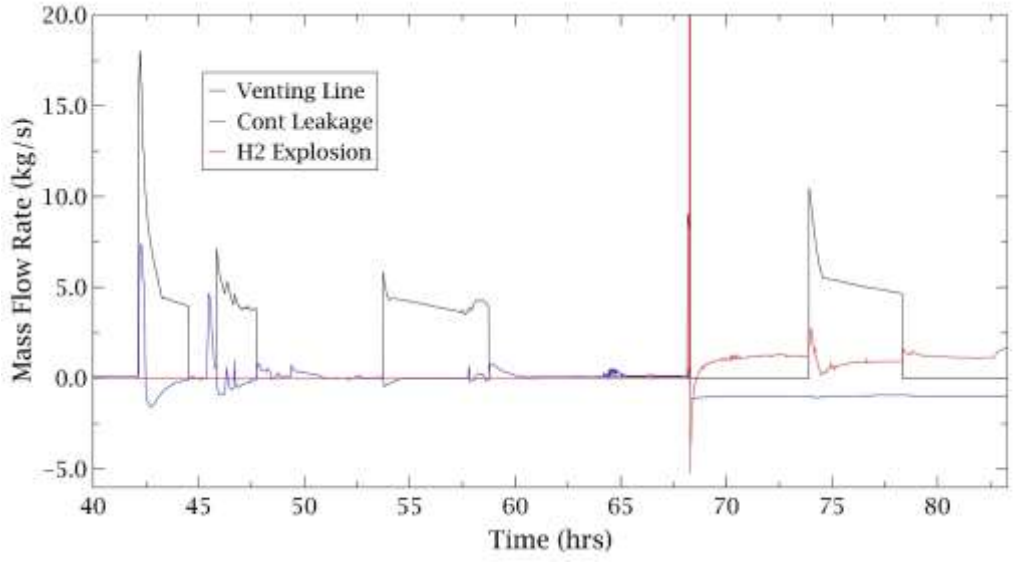

Figure 22 - Mass flow rate to environment

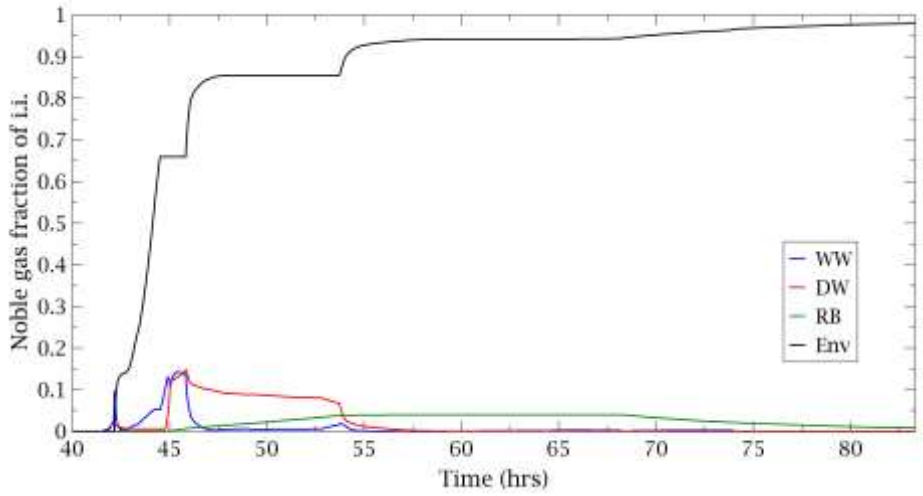

Figure 23 - Noble gas fraction to WW, DW, Reactor Building, Environment

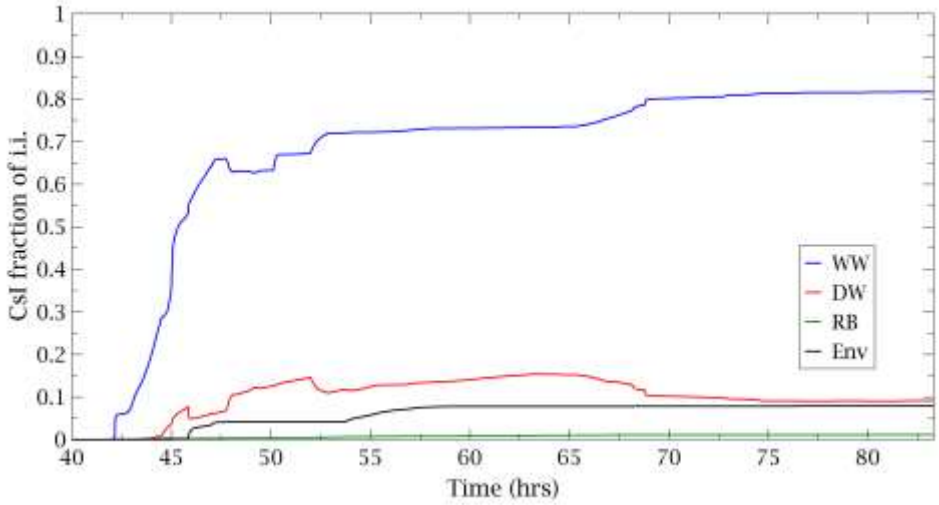

Figure 24 - CsI fraction to WW, DW, Reactor Building, Environment

CsI is effectively scrubbed and retained in the WW since the first venting operation. Most of CsI released in the environment comes from the second and third venting line operation in this calculation. The explosion at 68 h 15 min has no impact on further releases, likely underestimating the total source term. This is because MELCOR lacks a model for resuspension of deposited aerosols following an explosion. At the end of calculations, about 7.9% of CsI is released to the environment (Figure 24). Due to the complete reaction with Cs assumption (before the release), this is the same fraction of I source term. Cs released in environment is 1.0% of i.i. In Table 9 the distribution of mains radionuclides in WW, DW, RB and environment (Env) is reported in terms of initial inventory fraction. The Cs fraction has been evaluated considering the mass of Cesium forming CsOH, CsI, and CsM.

Table 9 - Distribution of RNs at the end of calculation (% of i.i.)

	Noble gases	Cs	I
WW	0.0	54.0	81.7
DW	0.0	5.2	9.1
RB	0.8	0.2	1.1

Env	98.0	1.0	7.9

The time and magnitude of release are still uncertain. Table 10 shows TEPCO estimates of radioactivity release for Unit 1, 2 and 3 between March 12th and March 31st, 2011 (TEPCO, 2012c). Fukushima Daiichi Unit 3 NPP was estimated to have released about 40% of the total source term (Cardoni et al., 2014a). Results of this MELCOR model are in good agreements with TEPCO and other studies (IAEA, 2015), considering different time range of calculation.

Table 10 - Radioactivity released in the environment calculation and estimates

	TEPCO calculation Unit 1-3	**TEPCO estimate Unit 3**	**Sapienza calculation Unit 3**
Cs-137	~10	~4	2.4
Cs-134	~10	~4	2.5
I-131	~500	~200	185
INES I-131equivalent	~900	~360	281

4 Variables and sampling

A Python script has been developed to allow the interaction between RAVEN and MELCOR (D'Onorio et al., 2020). The Python interface allows to perturb all the parameters accessible through the MELCOR input deck. The interface has three manly functions, interpret the information coming from RAVEN, translate such information in the input of the driven code and manipulate output data file to create a database. Figure 25 shows the procedural framework used for the uncertainty quantification. A MELCOR input deck is used as a template, the chosen parameters are specified as strings with special characters. In such a way, RAVEN can identify such parameters and replace the string with values sampled from a specified distribution. Consequently, number N of MELCOR input decks, specified in the sampling phase, is generated. Once the HDF5 database has been generated, statistical analysis of the output sets can be performed.

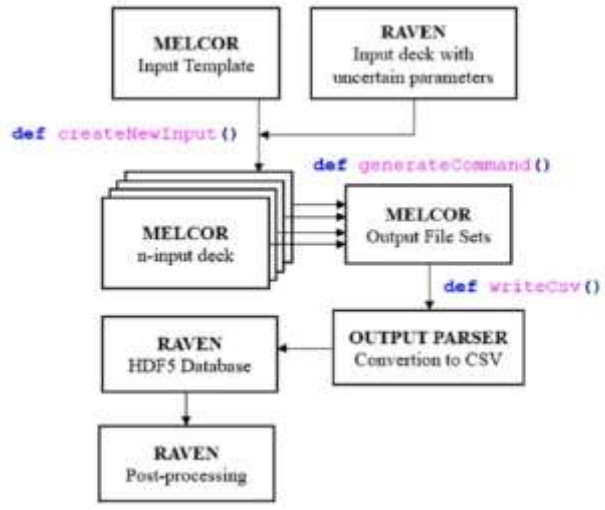

Figure 25 - MELCOR/RAVEN interface

4.1 Selected uncertainty parameters

A preliminary set of 15 uncertainty parameters have been selected for this analysis. The selected parameters are known to mainly affect the timing of cladding failure, fuel rod failure, hydrogen generation, melt relocation in core (radial and lateral spreading) and refreezing behaviour of draining molten core materials (Gauntt and Mattie, 2016).

Once all the variables have been selected a sampling strategy needs to be employed. The sampling strategy is used to perturb the input space in relation to variable distributions. The sample size needed to obtain a significative output statistic was selected using the Wilks formula for two-sided statistical tolerance limits (Wilks, 1941). The required minimum number of computer code calculations becomes 93 for a 95% probability and 95% confidence level (Glaser, H. 2008). In the present analysis, the Monte Carlo sampling strategy has been selected, setting a limit of 250 calculations to consider possible code failures. The list of perturbed parameters is reported in Table 11 together with the used distribution.

MELCOR sensitivity coefficient SC1020 is related to radial relocation rates of molten and solid debris because of gravitational effects. The relocation rates have times constants, which default values are 60 s for molten debris SC1020(2) and 360 s for solid debris SC1020(1). A uniform distribution was chosen since there is no reason to believe that the default is the central tendency of a distribution. Because the technical base for time constants values were insufficient, boundaries of these uncertainty parameters were selected based on the order of magnitude: 10-100s for molten debris radial relocation time constant and 100-1000s for solid debris radial relocation time constant (Bixler et al., 2016; Humphries et al., 2017).

Several perturbed parameters are related to the Zirconium alloy behaviour inside the reactor. The Zircaloy breakout temperature (SC1131) controls retention of molten zircaloy within ZrO_2 shell till oxide breakout temperature. The relocation of the oxidizing melt has the effect of terminating the intense local fuel heating, since the chemical heating source has relocated to a cooler region of the vessel, affecting hydrogen generation and fission products release. The lower bound for this parameter was set to Zr melting temperature (2100 K), the upper bound was set to 2540 K based on qualitative consideration of the alpha-Zr(O) phase diagram and observations/analyses of the Phebus experiments (Bixler et al., 2016, Cardoni et al., 2014b). The normal distribution suggests a most probable value of 2350 K, as used in SOARCA uncertainty analysis, with decreasing likelihood for values away from the most probable.

The Maximum melted Zirconium flow rate per unit width after breakthrough can be specified in MELCOR as sensitivity coefficient SC1141(2). This parameter controls the maximum drainage rate per unit surface width (kg/m-s) of molten pool after breakthrough of flow blockage or molten material released after clad oxide shell breakout. Since this parameter could affect in-vessel accident progression, it has been selected for this analysis. Mean value was set as SOARCA best-practice value of 0.2 kg/m-s, determined by CORA-13 experiment, with uniform distribution and exploratory bounds of 0.1 kg/m-s and 2 kg/m-s, since there is no basis to inform distribution bounds (Ross et al., 2014; Bixler et al., 2016).

Concerning the Zircaloy oxidation phenomenon, the parabolic rate constant of Zr reaction with steam, K_p, is related to temperature by $K_p = A \exp(-E/RT)$. Sensitivity coefficients SC1001(3) and SC1001(4) are

representative constant coefficient A and exponential coefficient E/R, respectively. In this sensitivity analysis a normal distribution centred on default value and standard deviation of 20% has been used for both SCs.

After zirconium melting and candling by exceeding breakout temperature there will be UO2/ZrO2 eutectic reactions forming complex U-Zr-O mixture having lower melting temperature than either ZrO2 or UO2. Temperature formation of eutectic could affect fuel failure and molten pools generation. The temperature at which eutectic will melt, could be changed in MELCOR by varying the SC1132(1) and ZrO2/UO2 melting temperatures in MP_PRC record. VERCORS test results show a mean fuel collapse temperature of 2479 K with a standard deviation of 83 K (Bixler et al., 2016, Pontillon et al., 2005).

The Zircalloy candling heat transfer coefficients affect the freezing of relocating molten material as zircaloy and steel, and thus the tendency to form blockage. A uniform distribution has been used with a lower bound of 7500 W/m^{2}K and an upper bound of 20000 W/m^{2}K, basing on SOARCA and SANDIA Uncertainty Analysis in (Gauntt et al., 2014). It should be noted that use of a high heat transfer coefficient does not result in the freezing of a large mass with resulting complete blockage, unless a sufficient heat sink is available to absorb the latent heat (i.e. clad, pellets, influenced by the thermal resistance of gap).

Particulate Debris (PD) parameters, like hydraulic diameter, porosity and fall velocity, have been perturbed since they could affect heat transfer and oxidation surface areas during in-vessel phase of accident. PD hydraulic diameter may be specified separately for core and lower plenum regions, where debris arrives melted, conglomerated or finely fragmented. When core collapses due to the loss of supporting structures or due to temperatures-threshold criteria, MELCOR converts fuel rods in PD, that relocates and fills available space, limited by debris porosity. In the core region seems reasonable a PD size having the same order of magnitude of fuel pellets diameter, that is about 1cm. Smaller values are possible due to fragmentations, larger values are possible due to sintered agglomerates (Pellegrini et al., 2016). In this work, the distribution for PD hydraulic diameter in core region has been set as uniform, with a lower bound of 0.5 cm and an upper bound of 2 cm. Instead, in the lower plenum PD hydraulic diameter distribution was set as uniform with lower bound 2 mm, upper bound 5 mm (Magallon et al., 2006).

In MELCOR, debris are assumed to fall toward the lower plenum with a user-specified velocity (VFALL) losing heat to the surrounding water. A uniform distribution has been set for this input parameter, ranging from SOARCA recommended value of 0.01 m/s, to the default MELCOR 2.1 users guide value of 1 m/s.

A normal distribution with mean at 0.4 and sigma 10% of mean value was used for the debris porosity. Greater porosity cannot be considered structurally stable, and lesser porosity cannot reasonably be achieved by random packing of solid debris particles.

During debris relocation to the lower plenum, a heat transfer coefficient from in-vessel falling debris to pool (HDBH2O) must be defined. This, together with falling velocity and debris hydraulic diameter, are the main parameters governing quenching of debris relocating into the lower plenum, influencing RPV thermal-hydraulic behaviour after core slumping. A review of FARO data shows that for fragmented particle sizes on the order of 5 mm, the HTC may be 1000 W/m^{2}K (Bixler et al., 2016). SOARCA suggest 2000 W/m^{2}K for debris size of 2 mm (Ross et al., 2014). A uniform distribution has been selected with these two values as bounds.

The debris quenching model also affects the initial temperature response of debris in the lower plenum and is therefore important for the subsequent calculations of RPV lower head response: once debris relocates to the lower head, it increases its temperature based on debris-lower head heat transfer coefficient, input in MELCOR code as HDBLH. The default heat transfer coefficients are order-of-magnitude parameters that should be varied in sensitivity studies to determine their impact on lower head heat transfer and failure. A uniform distribution is used, with bounds spanning from SOARCA recommended value of 100 W/m^2K and default value of 1000 W/m^2K.

5 Main results and outcomes

The results obtained with the perturbation of the degradation models' parameters have been statistically analyzed through the RAVEN post-processor. A dynamic statistical analysis has been performed setting time as pivot parameter. To give a better visualization of the calculated uncertainty bands, the 0.05, 0.5 (median) and 0.95 quantiles have been selected, analyzing the following FOMs. A direct comparison with the errors associated to the quantities measured is not carried out, due to the unavailability of these. For this, the comparison will be only with the available measured values.

Table 11 – Uncertainty parameters

Variable	Description	Distribution	Units	Parameters	LB	UB
SC1020 (1)	Time constant for the relocation of solid material	Uniform	s	-	100	1000
SC1020 (2)	Time constant for the relocation of molten material	Uniform	s	-	10	100
SC1131 (2)	Maximum ZrO2 temperature permitted to hold up molten Zr in clad (break-through temperature)	Normal	K	μ =2350 σ = 235	2100	2540
SC1141 (2)	Maximum melt Zr flow rate per unit width after breakthrough	Uniform	kg/m-s	-	0.1	2
SC1001(3)	Zircaloy Oxidation Rate Constant Coefficients - High temperature range constant coefficient	Normal	kg2/m4-s	μ =87.9 σ =17.58	65	110
SC1001(4)	Zircaloy Oxidation Rate Constant Coefficients - High temperature range exponential constant	Normal	K	μ =16610 σ =3322	12500	20000
SC1132 (1)	Effective temperature at which the eutectic formed from UO2 and ZrO2 melts	Normal	K	μ =2479 K σ = 83 K		
SC1132 (2)	Temperature at which fuel rods will fail, regardless of composition of the cladding	Uniform	K	-	2700	3100
HFRZZR	Candling heat transfer coefficient for Zr	Uniform	kg/m2-s	-	7500	20000
DHYPD core	Particulate debris equivalent diameter in core region	Uniform	m	-	0.005	0.02
DHYPD lp	Particulate debris equivalent diameter in lower plenum region	Uniform	m	-	0.002	0.005
VFALL	Velocity of falling debris	Uniform	m/s	-	0.01	1
PORDP	Porosity of particulate debris	Normal	-	μ = 0.4 σ = 0.04	0.3	0.5
HDBH2O	HTC from in-vessel falling debris to pool	Uniform	W/m2-K	-	1000	2000
HDBLH	Heat transfer coefficient from debris to lower head	Uniform	W/m2-K	-	100	1000

To quantify the linear correlation between the variables, the Pearson's coefficient has been used. It is defined between -1 and 1 and it measures the strength of the linear relationship between two variables.

All uncertainty parameters selected are known to affect core degradation and subsequent consequence, so they do not influence accident progression till core degradation begins.

In Figure 26 median and quantile of water level in reactor vessel is shown. Core degradation and subsequent influence of uncertainty variables start right after ADS actuation (42:10). At this point, water level is under BAF. Perturbed parameters mainly affecting the interaction between corium and lower plenum have a weak influence on liquid level at this stage because it strongly depends indeed on early degradation phases, that is on core region.

At core plate failure due to thermo-mechanical stresses, predicted between 43 h 47 min and 45 h 24 min, corium slumps in lower plenum region, producing high grade of vaporization, with pressure spike in DW/WW/RPV and large water level drop, till lower plenum dryout predicted to falls in a band between 44 h 41 min and 52 h 25 min, with a median value of around 50 h.

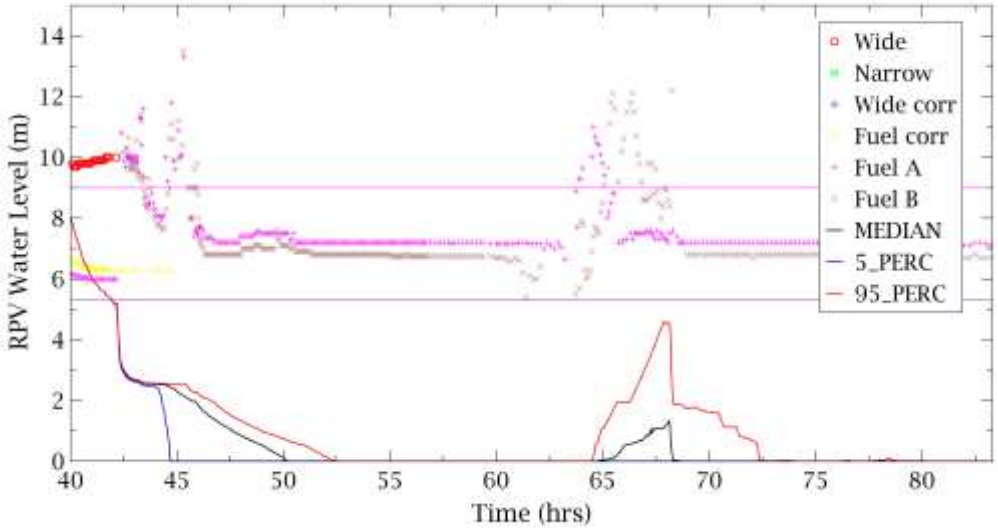

Figure 26 - Variation range of RPV liquid level

Fuel rods start to fail between 42 h and 44 h 37 min (Figure 27). Median of realizations suggests that some fuel assemblies remain intact, located on the outer ring of the core, where radial power factor are lowest. This is 26% of total mass, that is fuel mass located in ring 4 of MELCOR model. Parameters which have strong influence on fuel degradation are SC1132(1), SC1131(2) and SC1141(2). The Pearson coefficients are shown in Figure 28 and to evaluate the correlation between parameters and FOMs the classification made by Evans (1996) is used.

SC1132(1) Pearson coefficient has weak positive linear correlation at core degradation phase, with a maximum of 0.38. Since this parameter represent the Zr-U-O melting temperature that drives fuel rods fails, if this value increases means that fuel rods can stands at higher temperature without failing, so fuel intact fraction increases at its increasing.

SC1131(2), which sets the temperature at which fuel rods will fail break-through , has a (negative) moderate linear correlation with fuel intact fraction at later lower plenum degradation stage, due to a Pearson coefficient minimum value of -0.47 at 47 h 10 min. Once molten Zr breaches oxide shell and candles down, oxidation reaction

rate in that core cell decreases, lowering the rate of increase of temperature, thus extending the lifetime of that core zone. At higher breakout temperature corresponds higher fraction of oxidation degradation of local core zone, increasing rate of fuel rods failure, thus lowering the fuel intact fraction.

SC1141(2) governs maximum melt Zr flow rate per unit width after breakthrough. At higher flow rate corresponds higher mass of molten Zr relocating, thus lower local oxidation, temperature, and extended lifetime. It has a negative weak correlation at the core degradation stage, with Pearson coefficient minimum of -0.37 at 44 h 33 min.

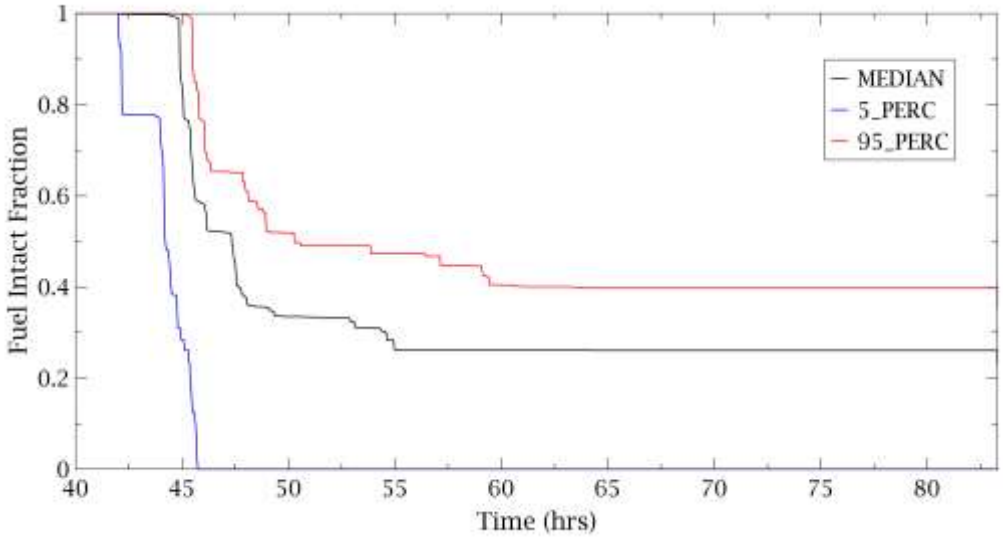

Figure 27 – Variation range of Fuel Intact Fraction

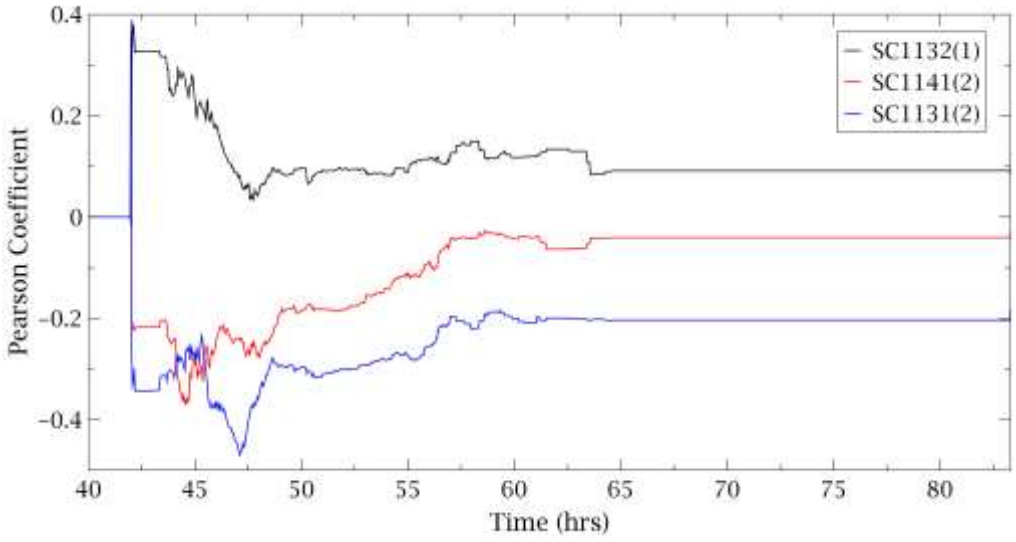

Figure 28 - Fuel Intact Fraction - Pearson coefficients

Figure 29 shows the range of hydrogen mass that could be produced perturbing the input parameters. At the end of calculations, a median value of 859kg was produced, with a mass ranging from 692 kg and 1053 kg of quantiles. Pearson coefficients of main uncertain parameters that affect hydrogen generation rate are shown in Figure 30. An increase of SC1131(2) contributes to higher mass of hydrogen produced, since higher Zr breakout temperature means higher degree of local oxidation for more time. Thus, Zr breakout temperature Pearson

coefficient has moderate positive correlation at first oxidation peak, with a maximum of 0.47. Furthermore, oxidation is an exponential function of temperature, so if oxidation can persist at higher temperature, more and more hydrogen is produced.

SC1141(2) has moderate linear correlation with hydrogen generation, with a maximum Pearson coefficient of 0.58 at core slumping. This coefficient governs maximum melt Zr flow rate per unit width after breakthrough. Hydrogen mass is an integral quantity and thus differs from its influence on core degradation, being related to a threshold fail temperature. In this case rising melt Zr available to oxidation, increases total H_2 mass produced, being not hold in a crust of oxidated Zr.

SC1020(1) sets time constant for the relocation of solid material τ_{spr}. Fraction of relocating solid material in time step Δt_c is $[1 - e^{(-\Delta t_c/\tau_{spr})}]$. So, it became higher at smaller τ_{spr}. Its Pearson coefficient related to hydrogen mass produced grows at corium slumping, keeps relatively steady, with a maximum of positive weak correlation (Pearson coefficient equal to 0.35) at later stages. It means that hydrogen mass is higher at smaller degree of relocating rate.

SC1001(4) sets Zr high temperature range exponential constant C oxidation rate. The rate constant for oxidation of Zircaloy as a function of temperature follows parabolic kinetics $K(T) \approx e^{-C/T}$. As expected, it has strongly negative correlation (a value of – 0.69 for the Pearson coefficient is reached during the firsts core degradation phases).

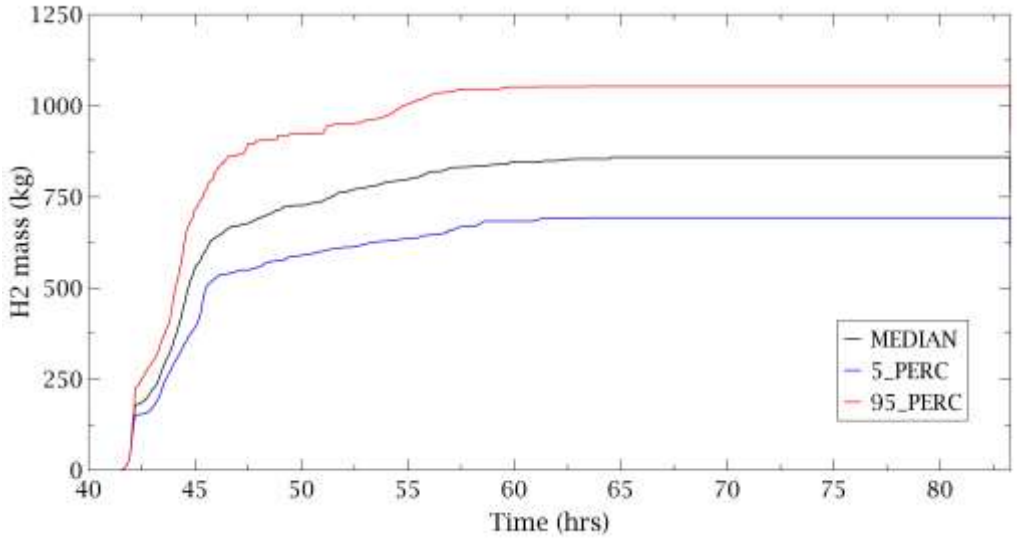

Figure 29 – Range of Hydrogen mass produced

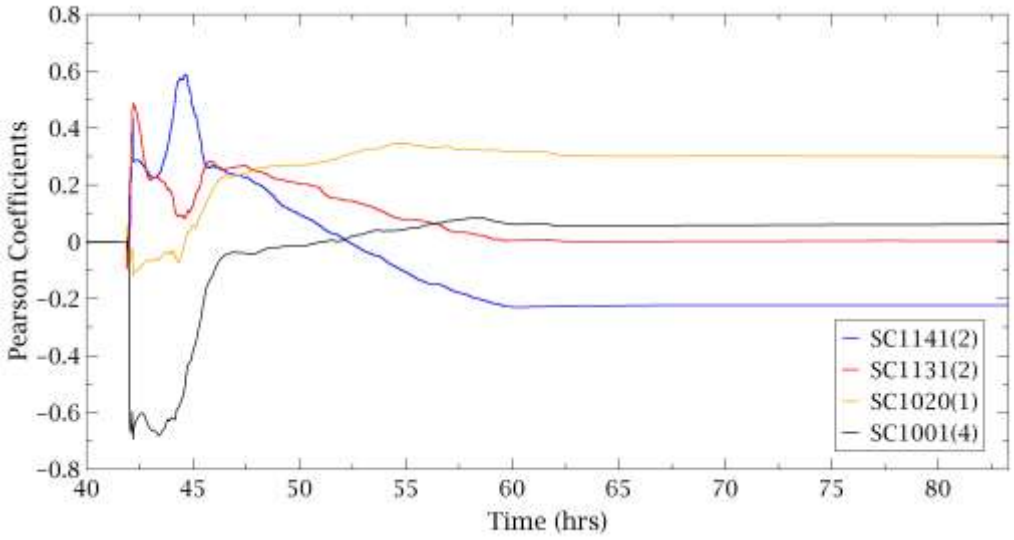

Figure 30 – Hydrogen mass produced - Pearson coefficients

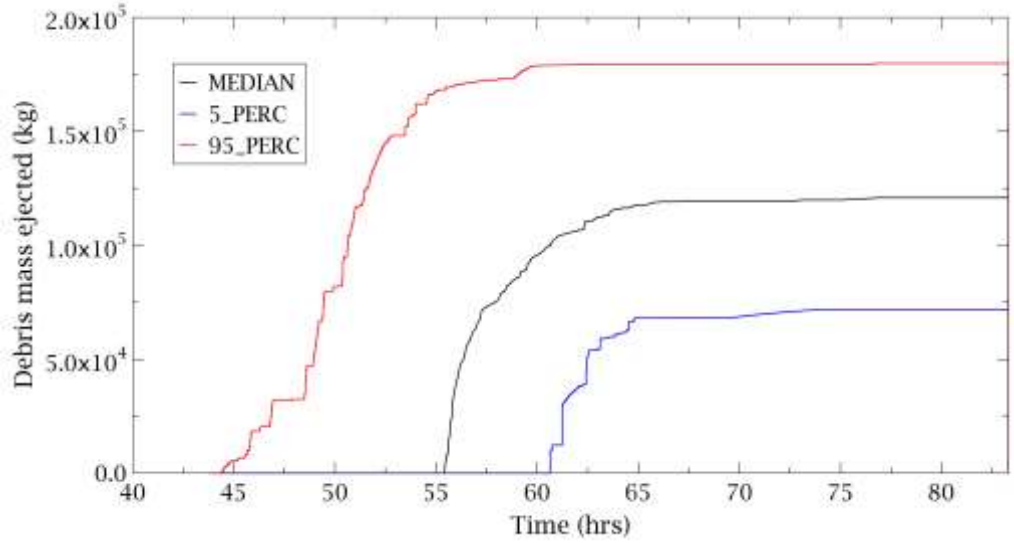

Figure 31 – Variation range of ejected debris mass

Total debris mass ejected after lower head failure (Figure 31) spans from 71900 kg to 179800 kg, with a median value of 120894 kg. Median of time of lower head creep is 55 h 27 min, with a 5% quantile of 44 h 27 min and 95% of 60 h 38 min. Lower head fails in all MELCOR runs.

Shown in Figure 32 is the spectrum of predicted DW pressure. The results of the calculated uncertainty band envelope mostly of the TEPCO plant data available related to the DW pressure.

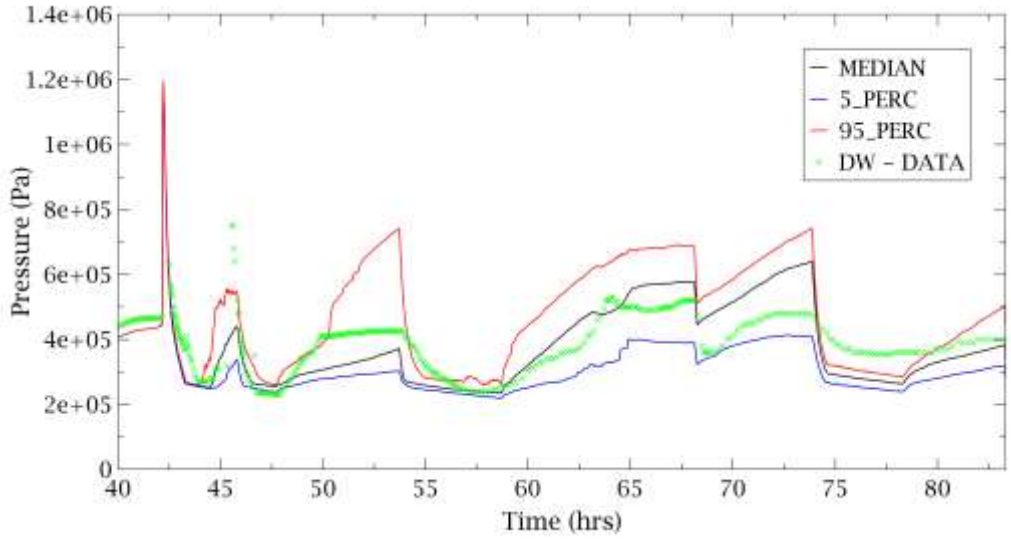

Figure 32 - DW pressure

This pressure is important relative to environment source term, that is influenced by SRVs, pumps leakage, WW/DW sprays and RPV pressure after ADS actuation, thus also responsive to core degradation, water level, freshwater, and seawater injection: it gives an almost complete view of the accident progression.

Main uncertainty parameters that affect DW pressure behaviour are maximum flow rate per unit surface width (kg/m-s) of molten Zr or molten pool set as SC1141(2), and Zr high temperature range exponential constant oxidation rate SC1001(4). Their correlation with DW pressure is shown in Figure 33.

Till corium slumping into the lower head, higher hydrogen mass produced by oxidation lead to higher pressure in RPV and because of ADS activation, in DW: SC1141(2) has Pearson coefficient peak of 0.37, SC1001(4) of -0.26. Both have a weak correlation with DW pressure at this stage.

At slumping, at about 45 h, less the Zr was already oxidated, greater will be available to oxidation during slumping, greater the pressure peak. Pearson coefficients invert signs, with SC1141(2) peak of -0.49, showing moderate negative correlation and weak SC1001(4) correlation with 0.37 as peak. Maximum Zr flow rate also sets behaviour of molten pool: its influence can be seen till lower head dry-out, when molten corium interacts with lower plenum water. SC1141(2) became again positive with weak correlation, because of corium oxidation with water/steam in lower plenum, increasing pressure at higher melt Zr flow rate.

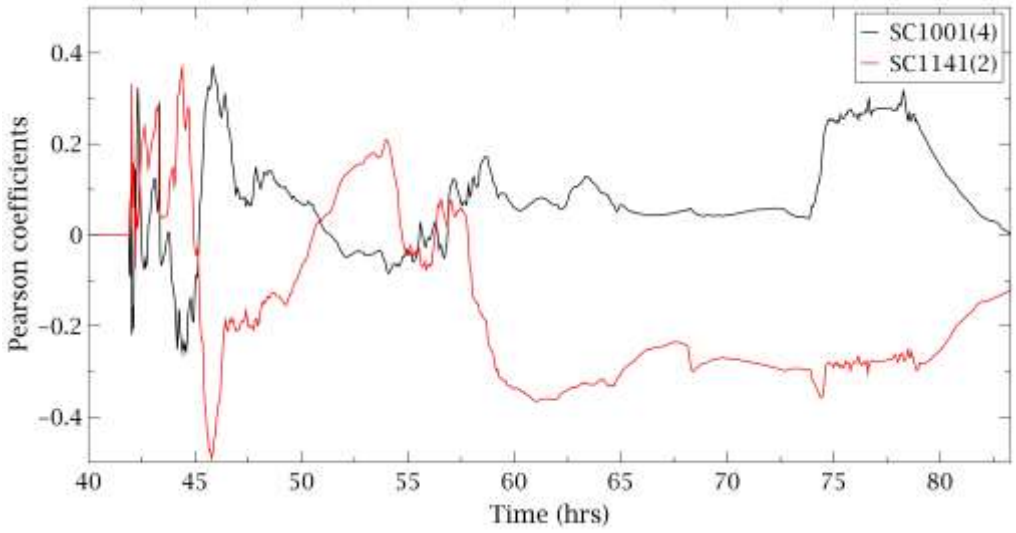

Figure 33 - DW Pressure - Pearson coefficients

Concerning the source term results, it should be noted that fission products release from fuel to the environment is a complex phenomenon, which mainly depends on fractional release from fuel, their chemical and physical behaviour during transient and path to environment. Results have shown that main releases timing is not affected by core degradation parameters, being fixed due to accident progression external triggering: venting remains main release path to environment. Containment leakage is negligible in this MELCOR model and explosion affects minimally only Noble gases release. However, the magnitude of release is affected by core degradation parameters.

As shown in Figure 34, fraction of Noble gases released in environment span from 95% to 100%, being almost totally released from fuel in all simulations and mostly released without any retention.

Release fraction of Caesium iodide spans from 6.2% to 11.8%, with a median value of 8.7% (Figure 35).

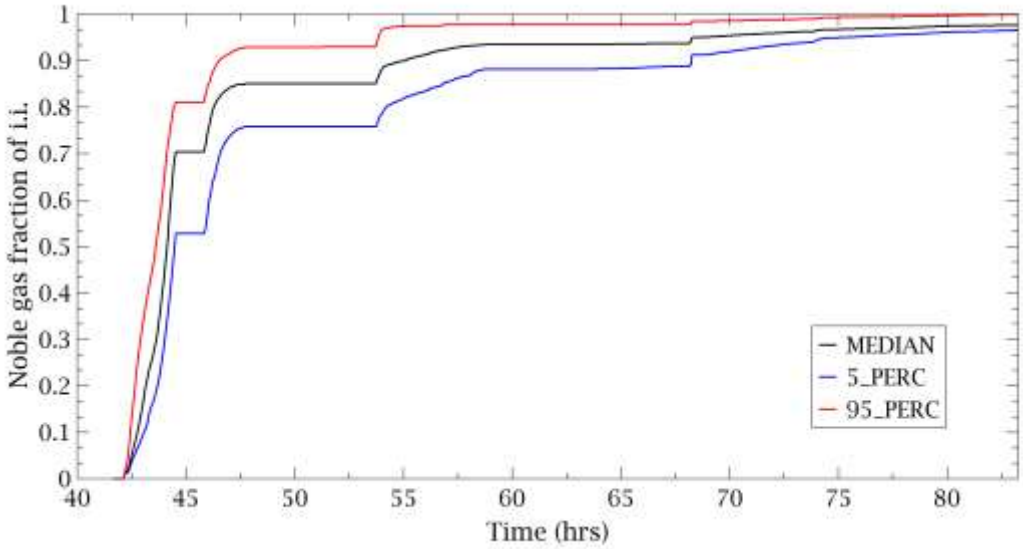

Figure 34 – Variation range of Noble gas released fraction

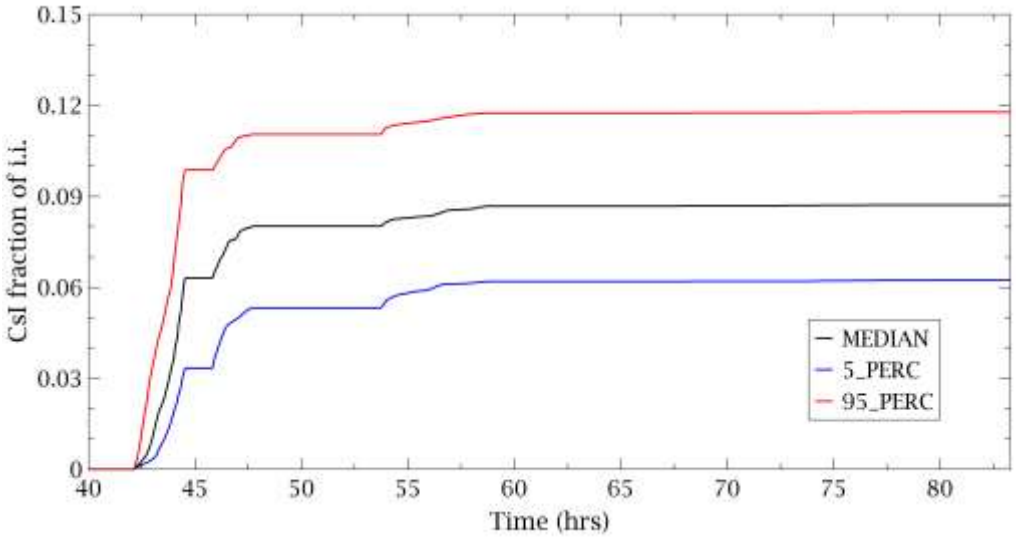

Figure 35 – Variation range of CsI released fraction

Most influent uncertainty parameter are:

- Maximum melt Zr flow rate per unit width after breakthrough SC1141(2). Relocation of Zr at higher rate makes available grater Zr mass to oxidize, increasing heat generation over a greater extend of area, thus promoting RNs release. This is also demonstrated by the Pearson coefficient which is positive with a moderate correlation of 0.54 maximum, right before corium slumping.
- Zircaloy breakout temperature SC1131(2) also shown positive Pearson coefficient and moderate correlation with CsI released fraction in first release phase, corresponding to the core zone degradation phase, with a maximum peak of 0.56. Relocation of oxidizing melt at higher temperature, delays interruption of local fuel heating, with higher temperature sustained for more time, thus increased RNs diffusivity and release.
- High temperature range exponential constant of Zircaloy Oxidation Rate Constant Coefficients SC1001(4) has strong negative correlation (Pearson coefficient 0.78 at core degradation phases) related to source term. Zircaloy oxidation rate increases at lower constant value that results in higher heat generation and higher fuel temperature, increasing RN release.

CsI source term fraction of i.i. depends mostly on venting operation, that is mean that most of CsI is released during the firsts core degradation phase (see Figure 36).

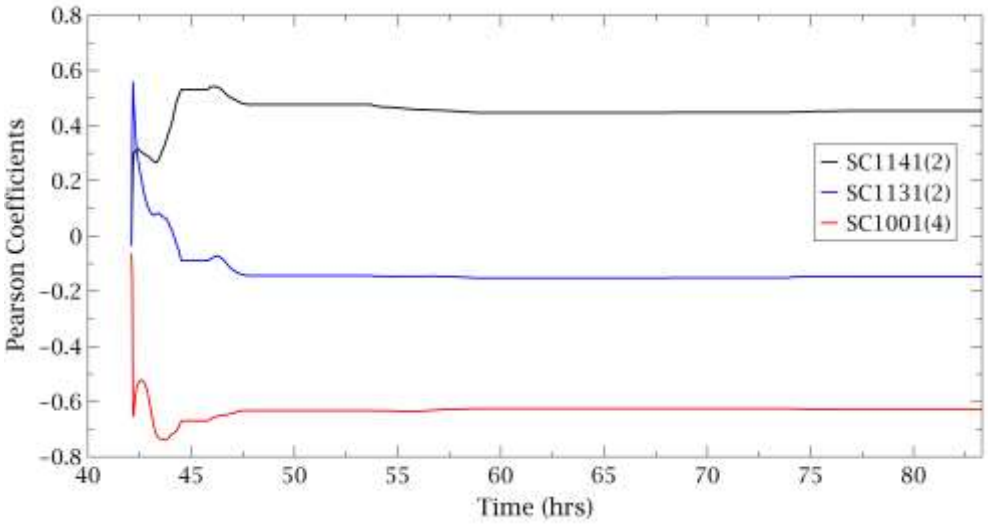

Figure 36 - CsI source term - Pearson coefficients

6 Conclusion and perspectives

A MELCOR model of BWR has been developed, taking as reference the Fukushima NPP Unit 3 reactor. The related accident scenario simulated with MELCOR 2.1 produced results in good agreement with TEPCO accident data and previous analyses found in the literature.

Starting from these results, a preliminary uncertainty of the code parameters related to core degradation behaviour has been performed. Main outcomes shown that core degradation phase is mainly influenced by ZrO2 break-through temperature, maximum melt Zr flow rate after break-through and Zircalloy oxidation rate coefficients. Median of realizations predicts about 1/4 of fuel assemblies remains intact on core outer periphery. This should be in agreement with TEPCO latest finds, which highlighted that part of core remained in core area. Base case predicts about 75% fuel failure, in accordance with the uncertainty analysis. Time span of dryout is from 45 h to 52 h. Data showed a likely time of lower plenum dryout consistent with calculations, from 53 h to 56 h, while base case predicts 52 h and 30 min.

MELCOR well predict lower head failure as found during TEPCO investigation. Investigation showed that part of debris is remained in the lower head, although massive and high-density material has not been found in RPV; part fells in PCV, showing that a breach exists. In the simulated base case scenario around 38% of core structures and fuel rods are retained in RPV, the remain 62% are relocated in PCV cavity.

Concerning source term results, Noble gases, Cs and I released fraction predicted by MELCOR are in good agreement with TEPCO and other literature data.

In conclusion, despite of existing parameters' uncertainty (final state not completely clear, thermohydraulic transient scenario not fixed and source term radioactivity measurements uncertainty) the developed MELCOR model shows good agreement with reactor accident data and the latest investigation scenario. Future uncertainty studies using MELCOR and RAVEN will be performed in the framework of the MUSA project with the same methodology and adding, when available, the comparison between the calculated code uncertainties and the correspondent experimental uncertainties.

Nuclear Engineering and Design 382 (2021), 111383 DOI:10.1016/j.nucengdes.2021.111383

List of Abbreviations

ADS	Automatic Depressurization System
AL	Axial Level
AO	Air Operated
AWI	Alternative Water Injection (
BWR	Boiling Water Reactor
CVH	Control Volume Hydrodynamics
CSS	Containment Spray System
CST	Condensate Storage Tank
DDFP	Diesel Driven Fire Pump
DW	Drywell
EDGs	Emergency Diesel Generators
FA	Fuel Assemblies
FoMs	Figures of Merit
HPCI	High Pressure Coolant Injection
JAEA	Japan Atomic Energy Agency
LP	Lower Plenum
MCCI	Molten Core-Concrete Interactions
MO	Motor Operated
MOX	Uranium Mixed Oxide
MSIVs	Main Steam Line Isolation Valves
PCV	Primary Containment Vessel
PD	Particulate Debris
RB	Reactor Building
RCIC	Reactor Core Isolation Cooling
RPV	Reactor Pressure Vessel
SFP	Spent Fuel Pool
SOARCA	State-of-the-Art Reactor Consequence Analyses
SNL	Sandia National Laboratories
SRV	Safety Relief Valve
TAF	Top Active Fuel
U.S.NRC	United States Nuclear Regulatory Commission
WW	Wetwell

References

Bixler, N.E., Ross, K., Sallaberry, C., Jones, J.A., Ghosh, S.T. 2016. State-of-the-Art Reactor Consequence Analyses Project: Uncertainty Analysis of the Unmitigated Short-Term Station Blackout of the Surry Power Station. https://www.osti.gov/servlets/purl/1380180

Cardoni J., Kalinich D. 2014a. Fukushima Daiichi Unit 1 Uncertainty Analysis - Preliminary Selection of Uncertain Parameters and Analysis Methodology. SAND2014-1170. https://doi.org/10.2172/1204089

Cardoni, J., Gauntt, R., Kalinich, D., Phillips, J., 2014b. MELCOR simulations of the severe accident at Fukushima Daiichi Unit 3. Nucl. Technol. 186:2, 179-197. https://doi.org/10.13182/NT13-41

D'Onorio, M., Giannetti, F., Porfiri, M.T., Caruso, G. 2020, Preliminary sensitivity analysis for an ex-vessel LOCA without plasma shutdown for the EU DEMO WCLL blanket concept, Fusion Eng. Des. 158, 111745, https://doi.org/10.1016/j.fusengdes.2020.111745

Evans R.H. 1996, An analysis of criterion variable reliability in conjoint analysis. Perceptual and Motor Skills, 82, 988-990

Fernandez-Moguel, L., Rydl, A., Lind, T. (2019a). Updated analysis of Fukushima unit 3 with MELCOR 2.1. Part 1: thermal-hydraulic analysis. Ann. Nucl. Energy 123, 59-77. https://doi.org/10.1016/j.anucene.2018.09.008

Fernandez-Moguel, L., Rydl, A., Lind, T. (2019b). Updated analysis of Fukushima Unit 3 with MELCOR 2.1. Part 2: Fission product release and transport analysis. Ann. Nucl. Energy 130, 93-106. https://doi.org/10.1016/j.anucene.2019.02.017

Gauntt, R.O., Kalinich, D., Cardoni, J., Phillips, J., Goldmann, A., Pickering, S., Francis, M., Robb, K., Ott, L., Wang, D., Smith, C., St. Germain, S., Schwieder, D., Phelan, Ch., 2012. FUKUSHIMA DAIICHI: ANS Committee Report, Fukushima Daiichi Accident Study (Status as of April 2012). SANDIA REPORT SAND2012-6173. Sandia National Laboratories, Albuquerque, New Mexico 87185 and Livermore, California 9455. https://doi.org/10.2172/1055601

Gauntt, R.O., Bixler, N., Wagner, K.C. 2014. An Uncertainty Analysis of the Hydrogen Source Term for a Station Blackout Accident in Sequoyah Using MELCOR 1.8.5. SANDIA REPORT SAND2014-2210. https://doi.org/10.2172/1200657

Gauntt, R.O., Mattie, P.D. 2016. Fukushima daiichi unit 1 accident progression uncertainty analysis and implications for decommissioning of Fukushima reactors – volume I. SANDIA REPORT SAND2016-0232, Sandia National Laboratories, Albuquerque, New Mexico. http://prod.sandia.gov/sand_doc/2016/160232.pdf

Hoshi, H., Ogino, M., Kawabe, R., Fukasawa, M. (2013). Computational analysis on accident progression of Fukushima Dai-ichi NPS. Proceedings of the PSAM topical conference in Tokyo (PSAM2013). Ref.ID 45084668.

Humphries, L.L., Beeny, B.A., Gelbard, F., Louie, D.L., Phillips, J., (2015). MELCOR Computer Code Manuals, Vol. 1: Primer and Users' Guide, Version 2.1.6840, SANDIA REPORT SAND-2015-6691R, Sandia National Laboratories, Albuquerque, New Mexico. https://www.nrc.gov/docs/ML1704/ML17040A429.pdf

Humphries, L.L., Beeny, B.A., Gelbard, F., Louie, D.L., Phillips, J., (2017). MELCOR Computer Code Manuals, Vol. 2: Reference Manual, Version 2.1.6840, SANDIA REPORT SAND2017-0876O, Sandia National Laboratories, Albuquerque, New Mexico. https://www.nrc.gov/docs/ML1704/ML17040A420.pdf

IAEA, 2015. The Fukushima Daiichi Accident - Technical Volume 1/5 - Description and Context of the Accident, https://www-pub.iaea.org/MTCD/Publications/PDF/AdditionalVolumes/P1710/Pub1710-TV1-Web.pdf

ICANPS. (2012). Final Report Investigation Commitee on the Accident of Fukushima Nuclear Power Stations of Tokyo Electric Power Company. Available at https://www.cas.go.jp/jp/seisaku/icanps/eng/final-report.html

Lind, T., Pellegrini, M., Herranz, L.E., Sonnenkalbd, M., Nishi, Y., Tamaki, H., Cousin F., Fernandez Moguel, F, Andrews, N., Sévon, T. 2021. Overview and outcomes of the OECD/NEA benchmark study of the accident at the Fukushima Daiichi NPS (BSAF), Phase 2 – Results of severe accident analyses for unit 3. Nuclear Eng. Des. 376, 111138, https://doi.org/10.1016/j.nucengdes.2021.111138

Glaser, H. 2008. GRS Method for Uncertainty and Sensitivity Evaluation of Code Results and Applications. Science and Technology of Nuclear Installations 2008, 798901, https://doi.org/10.1155/2008/798901

Magallon D. 2006. Characteristics of corium debris bed generated in large-scale fuel-coolant interaction experiments. Nuclear Eng. Des. 236, 1998-2009. https://doi.org/10.1016/j.nucengdes.2006.03.038

Nishihara, K., Iwamoto, H., Suyama, K. 2012 Estimation of Fuel Compositions in Fukushima-Daiichi Nuclear Power Plant. Japan Atomic Energy Agency. https://doi.org/10.11484/jaea-data-code-2012-018

Pellegrini, M., Suzuki, H., Mizouchi, H., Naitoh, M., 2014. Early phase accident progression analysis of Fukushima Daiichi Unit 3 by the SAMPSON code, Nucl. Technology 186, 241–254, https://doi.org/10.13182/NT13-107

Pellegrini, M., Dolganov, K., Herranz Puebla, L.E., Bonneville, H., Luxat, D., Sonnenkalb, M., Ishikawa, J., Song, J.H., Gauntt, R.O., Fernandez Moguel, L., Payot, F., Nishi, Y., 2016. Benchmark Study of the Accident at the Fukushima Daiichi NPS: Best-Estimate Case Comparison. Nucl. Technology 196, 198-210. https://doi.org/10.13182/NT16-63

Pellegrini, M., Naitoh, M., Kudo, Y., Mizokami, S., 2019. Confirmation of severe accident code modeling in light of the findings at Fukushima Daiichi NPPs. Nuclear Eng. Des. 354, 110217. https://doi.org/10.1016/j.nucengdes.2019.110217

Pontillon, Y., Malgouyres, P.P., Ducros, G., Nicaise, G., Dubourg, R., Kissane, M., Baichi, M. 2005. Lessons learnt from VERCORS tests. Study of the active role played by UO2–ZrO2–FP interactions on irradiated fuel collapse temperature. Journal of Nuclear Materials 344, pp. 265–273 (2005). https://doi.org/10.1016/j.jnucmat.2005.04.053

Rabiti C., Alfonsi A., Cogliati J., Mandelli D., Kinoshita R., Sen S., Wang C., Talbot W.P., Maljovec D.P., Chen J. (2017). RAVEN User Manual, INL/EXT-15-34123. https://inldigitallibrary.inl.gov/sites/sti/sti/Sort_4450.pdf

Robb, K.R., Francis, M.W., Ott, L.J., 2014. Insight from Fukushima Daiichi Unit 3 investigations using MELCOR. Nucl. Technol. Vol, 186:2, 145-160. https://doi.org/10.13182/NT13-43

Ross, K., Phillips, J., Gauntt, R. O., Wagner, K.C., (2014). MELCOR Best Practices as Applied in the State-of-the-Art Reactor Consequence Analyses (SOARCA) Project, NUREG/CR-7008, U.S. NRC. https://www.nrc.gov/docs/ML1423/ML14234A136.pdf

Sevón, T., 2015. A MELCOR model of Fukushima Daiichi Unit 3 accident. Nucl. Eng. Des. 284, 80–90. https://doi.org/10.1016/j.nucengdes.2014.11.038

Sato, I., 2017. A Plant data evaluation for Fukushima-Daiichi NPP Unit 3. 2017 Fall Meeting of AESJ, Sapporo, Hokkaido, Japan, September 13–15th.

TEPCO. 2011. Fukushima Nuclear Accident Analysis Report (Interim Report). Tokyo: Tokyo Electric Power Company, Inc. December 2nd. Available at http://www.tepco.co.jp/en/press/corp-com/release/betu11_e/images/111202e14.pdf

TEPCO. 2012a. Fukushima Nuclear Accident Analysis Report. Tokyo: Tokyo Electric Power Company, Inc. http://www.tepco.co.jp/en/press/corp-com/release/2012/1205638_1870.html

TEPCO. 2012b Estimation of the Released Amount of Radioactive Materials into the Atmosphere as a Result of the Accident in the Fukushima Daiichi Nuclear Power Station. Tokyo: Tokyo Electric Power Company, Inc. https://www.tepco.co.jp/en/press/corp-com/release/betu12_e/images/120524e0205.pdf

TEPCO. 2012c. MAAP Code-Based Analysis of the Development of the Events at the Fukushima Daiichi Nuclear Power Station. Tokyo: Tokyo Electric Power Company, Inc. https://f-archive.jaea.go.jp/dspace/handle/faa/12619

TEPCO. 2013a. Reactor pressure decreasing behavior at about 9:00 on March 13th in Unit-3. https://www.tepco.co.jp/en/press/corp-com/release/betu13_e/images/131213e0121.pdf

TEPCO, 2013b. Leakage from B Area South Tank. Tokyo Electric Power Company Online Report. Tokyo Electric Power Company, Tokyo. https://www.tepco.co.jp/en/nu/fukushima-np/handouts/2013/images/handouts_131003_01-e.pdf

TEPCO, 2013c. Result of Radioactive Nuclide Analysis around Fukushima Daiichi Nuclear Power Station. Tokyo Electric Power Company, Tokyo. http://www.tepco.co.jp/en/nu/fukushima-np/f1/smp/2013/index03-e.html

TEPCO. 2017. Locating Fuel Debris inside the Unit 3 Reactor Using a Muon Measurement Technology at Fukushima Daiichi Nuclear Power Station. TEPCO Holding, Tokyo. https://www.tepco.co.jp/en/nu/fukushima-np/handouts/2017/images/handouts_170928_01-e.pdf

Wilks, S.S. 1941. Determination of sample sizes for setting tolerance limits. Ann. Math. Stat., 12 (1941), pp. 91-96. https://doi.org/10.1214/aoms/1177731788

Yanez J, et al., An analysis of the hydrogen explosion in the Fukushima-Daiichi accident, International Journal of Hydrogen Energy (2015), http://dx.doi.org/10.1016/j.ijhydene.2015.03.154